PHILOSOPHICAL TRANSACTIONS B

royalsocietypublishing.org/journal/rstb

Review

Cite this article: Adamatzky A. 2019 A brief history of liquid computers. *Phil. Trans. R. Soc. B* **374**: 20180372.
http://dx.doi.org/10.1098/rstb.2018.0372

Accepted: 26 November 2018

One contribution of 15 to a theme issue 'Liquid brains, solid brains: How distributed cognitive architectures process information'.

Subject Areas:
bioengineering

Keywords:
liquid, fluidics, sensing

Author for correspondence:
Andrew Adamatzky
e-mail: andrew.adamatzky@uwe.ac.uk

A brief history of liquid computers

Andrew Adamatzky

Unconventional Computing Lab, Department of Computer Science and Creative Technologies, University of the West of England, Bristol, UK

AA, 0000-0003-1073-2662

A substrate does not have to be solid to compute. It is possible to make a computer purely from a liquid. I demonstrate this using a variety of experimental prototypes where a liquid carries signals, actuates mechanical computing devices and hosts chemical reactions. We show hydraulic mathematical machines that compute functions based on mass transfer analogies. I discuss several prototypes of computing devices that employ fluid flows and jets. They are fluid mappers, where the fluid flow explores a geometrically constrained space to find an optimal way around, e.g. the shortest path in a maze, and fluid logic devices where fluid jet streams interact at the junctions of inlets and results of the computation are represented by fluid jets at selected outlets. Fluid mappers and fluidic logic devices compute continuously valued functions albeit discretized. There is also an opportunity to do discrete operation directly by representing information by droplets and liquid marbles (droplets coated by hydrophobic powder). There, computation is implemented at the sites, in time and space, where droplets collide one with another. The liquid computers mentioned above use liquid as signal carrier or actuator: the exact nature of the liquid is not that important. What is inside the liquid becomes crucial when reaction–diffusion liquid-phase computing devices come into play: there, the liquid hosts families of chemical species that interact with each other in a massive-parallel fashion. I shall illustrate a range of computational tasks, including computational geometry, implementable by excitation wave fronts in nonlinear active chemical medium. The overview will enable scientists and engineers to understand how vast is the variety of liquid computers and will inspire them to design their own experimental laboratory prototypes.

This article is part of the theme issue 'Liquid brains, solid brains: How distributed cognitive architectures process information'.

1. Introduction

A substance offering no resistance to shear deformation is a fluid. A liquid is an incompressible fluid. Following the overall theme of this special issue 'Liquid brains, solid brains', co-edited by Ricard Solé, Melanie Moses and Stephanie Forrest, I focus on computing devices where a liquid plays a key role, either as a material substance for signal representation and transmission or as a substrate where computation takes place. A liquid plays a key role in the functioning and behaviour of several creatures, discussed in this special issue. Thus, for example, slime mould *Physarum polycephalum* is well known for coordinated channelling of fluid through its networks of protoplasmic tubes [1–4]. There is evidence of signal propagation with cytoplasmic flow [5], including morphological changes triggered by the cytoplasmic flow [6]. The networks of biochemical oscillators governing the shuffling of cytoplasm in the slime mould could be also responsible for the slime mould's adaptive behaviour and learning [7–10]. At the level of social insect behaviour, fire ants exhibit fluid-like behaviour in their outbound traffic [11,12], and interactions between neighbouring ants in moving traffic could be seen as analogous to interaction between molecules in a fluid substrate [13].[1] My personal interest in liquid-based computers started in the early 1990s when I proposed a paradigm and experimental laboratory implementations of reaction–diffusion chemical computers [17,18],

THE ROYAL SOCIETY PUBLISHING

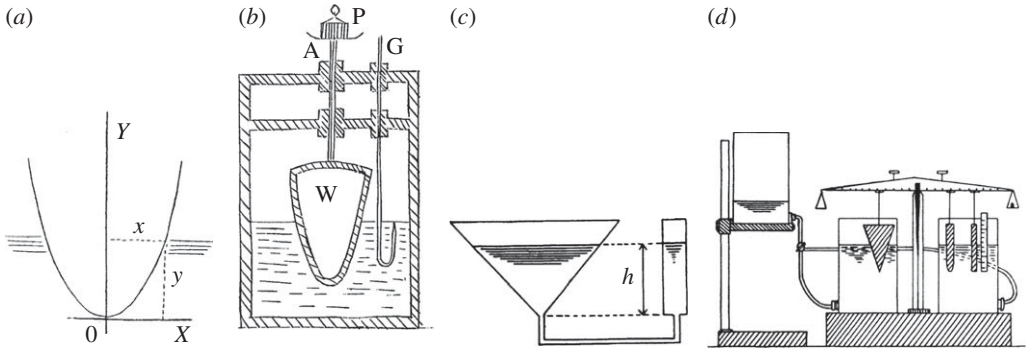

Figure 1. (*a*,*b*) Illustration of the hydraulic method for extracting the *n*th root of any number proposed by Arnold Emch in 1901. Adapted from [24]. (*c*,*d*) Pictures from [26].

affective liquids [19] and liquid brains for robots [20,21]. In reaction–diffusion computers, information is processed via interaction of phase or diffusion wave fronts. Affective liquids are mixtures of chemical species representing emotional states [19], and stirred or thin-layer mixtures of doxastic and affective chemical-like species [22]. Liquid brains for robots are onboard controllers for robot navigation that employ a thin-layer excitable chemical reaction [23].

Echoing one of the threads of this special issue—'a creature does not have to have a nervous system to cognize'—I demonstrate that a substrate does not have to be solid to compute. Liquid-based computing devices overlap with old schools analogue computation, as it was in the 1950s–1960s, and unconventional computation, as it fully flourishes in the 2000s. The field of analogue computation has been mainly populated by engineers and therefore most achievements have been highly practical. Unconventional computing, till recently, has been in the domain of computer science and therefore is full of theoretical papers. I estimate that for every thousand theoretical papers there is just one experimental laboratory paper. This is why an experimental laboratory prototype of an unconventional computing device is of utmost importance. Therefore in this paper I focus not on why a liquid can compute but on what practical computing devices can be made from liquid-phase substrates. I overview a variety of liquid computers, from hydraulic algebraic machines invented in the late 1890s to liquid marble logic designed just recently. The chronological order of selected liquid-based computing devices is shown in table 1. All the prototypes have only one thing in common: they use liquid to encode and process information. The exact implementations of the computing devices are very different one from another. Hydraulic mathematical machines employ mass transfer analogies; a fluid in such machines is mostly stationary except when bodies are immersed. Streams and jets of a fluid are employed in fluid mappers to explore geometrically constrained spaces and in fluid logic devices to realize logic gates via interaction of fluid jets. The streams are continuous. The liquid can also be 'discretized' in droplets and liquid marbles, and computation is implemented via liquid marbles colliding with each other or actuating mechanical devices. In hydraulic algebraic machines, integrators and droplet-based computers, the nature of the liquid is not critical because the liquid is used as an actuator or carrier of signals. What is inside the liquid becomes important when reaction–diffusion liquid-phase computing devices come into play: there, the liquid hosts families of chemical species that interact with each other in a massive-parallel fashion. Here I shall illustrate a range of computational tasks, including a computational geometry, implementable by oxidation wave fronts in nonlinear active chemical medium.

Table 1. A brief history of liquid computers.

year	device	publications
1900	hydraulic algebraic machines	[24–26]
1936	hydraulic integrators	[27,28]
1949	Monetary National Income Analogue Computer	[29]
1949	fluid mappers	[30]
1960[2]	fluidic logic	[32–36]
1985	Belousov–Zhabotinsky computers	[18,37–40]
1996	reaction–diffusion computers	[41–44]
2003	liquid brain for robots	[20,45]
2003	fluid maze solver	[46]
2007	droplet logic (pressure/flow-driven)	[47–50]
2010	chemotactic droplets solving mazes	[51,52]
2012	droplet logic	[53]
2017	liquid marbles logic	[54]

The examples discussed demonstrate the versatility of the liquid as a computing substrate. I believe the overview will encourage researchers and engineers to be more proactive in employing the liquid phase in their unconventional computing devices.

2. Hydraulic algebraic machines

The first recorded liquid computers worked on the displacement of water in response to immersion of a body in a container. In 1901, Arnold Emch published a paper in *The American Mathematical Monthly* where he proposed to calculate the *n*th root of any number by immersing solid bodies in a liquid [24]. He assumed a paraboloid-shaped body is immersed in liquid as shown in figure 1*a*. When this body is immersed, the weight of the displaced water will be $W = \pi \cdot w \cdot \int_0^y x^2\,\mathrm{d}y = \pi \cdot w \cdot \int_0^y x^2\,\mathrm{d}y$, where w is the weight of one cubic foot of water. The function $f(x)$ is selected such that the weight W of the displaced water equals the nth power of a given number y: $\pi \cdot w \cdot \int_0^y x^2\,\mathrm{d}y = y^n$.

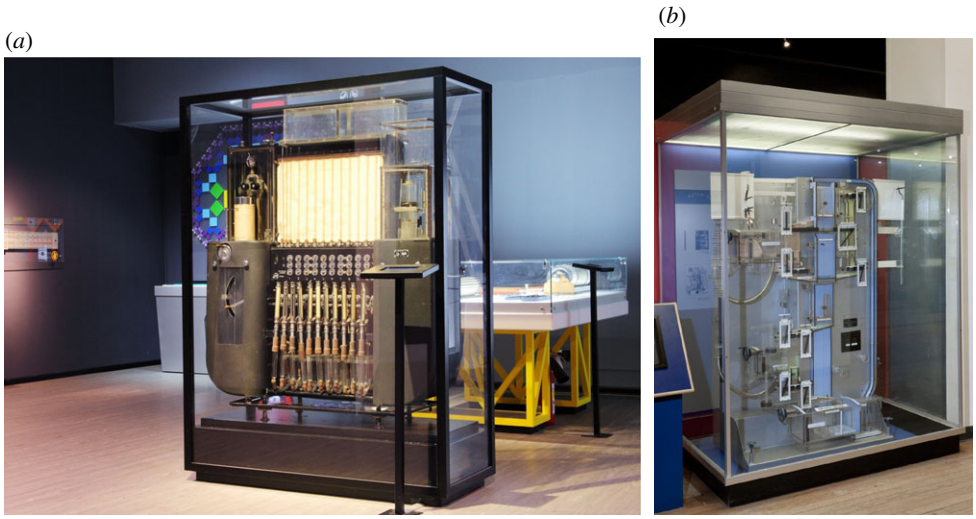

Figure 2. Hydraulic equation solvers. (*a*) Luk'yanov's hydraulic integrator (1936). This is a photo of Model no. 3 hydraulic integrator donated by the Ryazan Factory of Analog Computers to the Moscow Polytechnic Institute in 1956. Photo copyright © 2005–2018 Polytechnic Museum (Moscow, Russia). (*b*) Phillips Hydraulic Computer (1949). Science Museum Group Collection. Copyright © The Board of Trustees of the Science Museum. (Online version in colour.)

A device for the extraction of a square root of a given number N is shown in figure 1*b*. G is a hook-gauge showing the water level. The shape of the parabolic body immersed is defined by the equation $y = x^2 \cdot \sqrt{(\pi w)/2}$. Let W be the weight of the water displaced, Q be the weight of the vessel, and P be an added weight to make $Q \cdot P = N = y^2$. Thus, $y = \sqrt{N}$. The value y is measured by gauge G as the difference of the water levels before and after the immersion.

A method of solving trinomial equation $x^3 + x = c$, where c is a constant, was proposed by Demanet, cited by Gibb [26]. The device shown in figure 1*c* is an inverted cone joined to a cylinder, base 1 cm^2, with a tube. The height of the cone H and the cone's radius R are selected so that $R/H = \sqrt{3}/\sqrt{\pi}$. A volume c cm^2 of water poured into the device will stay at the height h in both vessels. The volume of the water in the cylinder will be $V = h^3$ (because $R = h \cdot (\sqrt{3}/\sqrt{\pi})$). The volume of the water in the cylinder used in the device is $1 \cdot h$. Thus, we have $h^3 + h = c$. The height h of the water is the solution of the equation.

A hydrostatic balance, inspired by Emch [24], was proposed by Meslin, cited in Gibb [26] to solve the equation $p \cdot x^m + q \cdot x^n + \ldots = A$ (figure 1*d* [26]). Solid bodies are immersed in a liquid. Parameters of the bodies are selected so that when x units of length are immersed in the liquid the volumes are proportional to x^m, x^n, …. Coefficients p, q, etc., are represented by distances of the bodies' hanging points relative to the axis of rotation of the beam (left means negative and right positive). After the bodies are immersed a weight $|A|$ is suspended at a unit distance from the axis of rotation. The system becomes temporarily disturbed but the equilibrium is restored by the water redistributing between the vessels. After that the moments of the bodies relative to the axis of rotation of the beam will be $p \cdot h^m + q \cdot h^n + \ldots$, and therefore h is the solution found.[3]

3. Hydraulic integrators

Flows of a liquid through a network of pipes with different diameters can analogously imitate thermal diffusion in geometrical constraint spaces, electrical conductivity and money flow in a country's economy. In the early 1930s, two hydraulic computing devices were invented simultaneously in the USSR by Luk'yanov [27] and in the USA by Moore [28]. Both were designed to imitate heat transfer not by solving differential equations by hand or using existing calculators but by analogue modelling of the heat propagation with water (figure 2*a*). The devices relied on the following analogies between the liquid and the thermal characteristics of thermo-conductive building materials [27,28,55]. Levels of water in vessels represent difference of temperatures between the building materials and the air. The cut area of the vessels represents the thermal capacity of layers. Hydraulic resistance of the tubes connecting the vessels is analogous to the thermal resistance of the simulated material layers.

As stated by the Polytechnic Museum (Moscow, Russia) [56], there were around 150 hydraulic integrators produced in the USSR, some exported to Poland, the Czech Republic and China. A portable version of the Luk'yanov integrator was manufactured for schools.

Over a decade after the invention and relatively wide usage of the hydraulic integrators, in the late 1940s, William Phillips designed and prototyped his Monetary National Income Analogue Computer (MONIAC), also known as the Phillips Hydraulic Computer (figure 2*b*). There, a flow of money was imitated by a redistribution of water between the containers [29].

4. Fluid mappers and maze solvers

A current in a liquid is strongest along the shortest path (or paths) from a source to a sink (or sinks). Fluid mappers visualize the current streams, thus extracting shortest paths from the liquid computers. In 1900, Hele-Shaw & Hay proposed an analogy between stream lines of a fluid flow in a thin layer and the lines of magnetic induction in a uniform magnetic field [57]. They applied their ideas to solve a 'problem of the magnetic flux distortion brought about by armature teeth' [58]. In the 1940s Hele-Shaw and Hay analogies were advanced by Arthur Dearth Moore, who developed fluid flow mapping devices [30].

The Moore's fluid mappers were made of a cast slab, covered by a glass plate, with input (source) and output (sink) ports. Crystals of potassium permanganate or methylene blue were evenly distributed at the bottom of the slab.

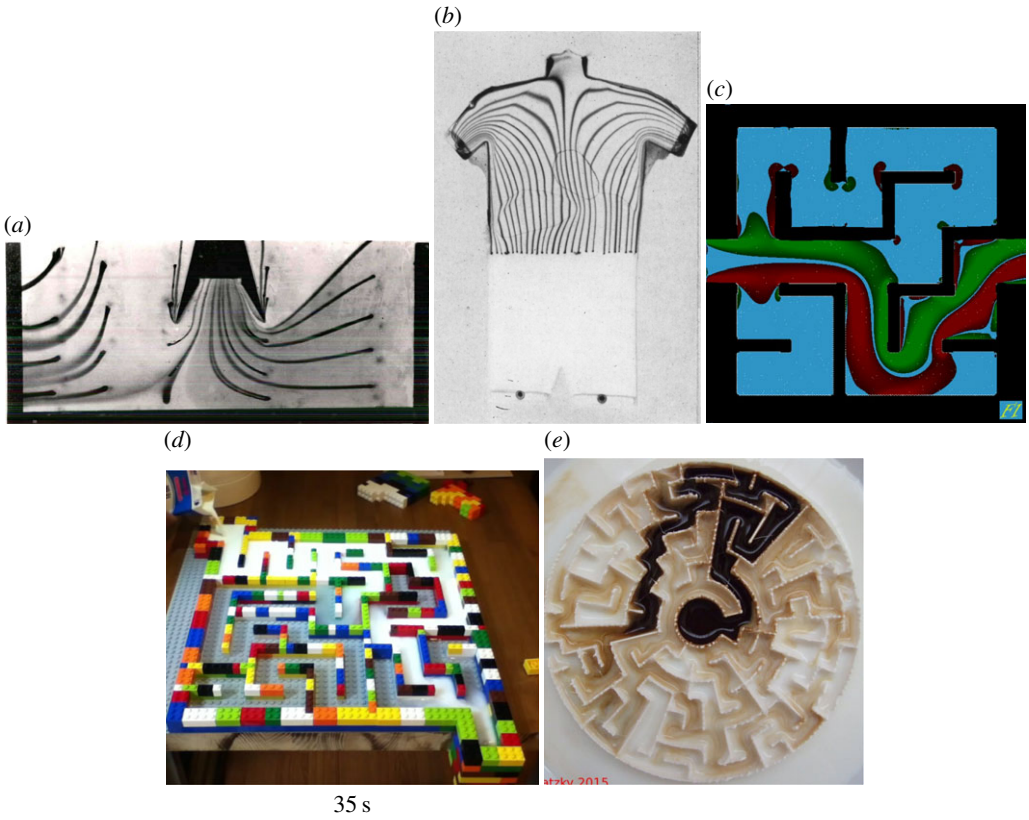

Figure 3. Fluid mappers and solvers. (*a*) A fluid mapper used in optimization of a canopy exhaust hood in 1954 [61]. (*b*) An imitation of the current flow in the human body by a thin-layer fluid flow, with domains of low permeability corresponding to the lungs and liver; the fluid enters the model from the left leg and leaves the model through the arms. The experiments were conducted in 1952. From [60]. (*c*) The fluid flow through a maze. The entrance is on the left; the exit is on the right. The flow simulation is done in Flow Illustrator http://www.flowillustrator.com/ for visual flow control $dt = 0.01$ and Reynolds number 500. The maze is black, red coloured areas are parts of the fluid making clockwise rotation and green coloured areas—counter-clockwise. (*d*) Maze solving with milk and water; snapshots from the video of experiments by Masakazu Matsumoto (https://youtu.be/nDyGEq_ugGo) with kind permission from Masakazu Matsumoto. (*e*) Labyrinth solving with coffee and milk: the path is traced by the coffee [62]. (Online version in colour.)

Fluid flow lines were visualized by traces from the dissolving crystals. Moore shown that the fluid mappers can simulate electrostatic and magnetic fields, electric current, heat transfer and chemical diffusion [30]. The fluid mappers became popular, for a decade, and have been used to solve engineering problems of underground gas recovery and canal seepage [58,59], current flow modelling in the human body [60] (figure 3*b*) and design of fume exhaust hoods [61] (figure 3*a*).

The Moore's fluid mappers could solve mazes; however, Moore never reported this. The first published evidence of an experimental laboratory fluid maze solver dates back to 2003. In the fluidic maze solver developed in [46], the maze is a network of micro-channels. The network is sealed. Only the source site (inlet) and the destination site (outlet) are open. The maze is filled with a high-viscosity fluid. A low-viscosity coloured fluid is pumped under pressure into the maze, via the inlet. Owing to a pressure drop between the inlet and the outlet, liquids start leaving the maze via the outlet. The velocity of the fluid in a channel is inversely proportional to the length of the channel. High-viscosity fluid in the channels leading to dead ends prevents the coloured low-viscosity fluid from entering the channels. The shortest path—least hydrodynamic resistance path—from the inlet to the outlet is represented by the channels filled with coloured fluid (figure 3*c*). A similar approach could be used to solve a maze at a macro scale, e.g. with milk and water (figure 3*d*) or milk and coffee (figure 3*e*).

5. Droplet-tracing fluid mappers

Current and chemical gradients in liquid computers can be traced with droplets of another liquid. We can think of this as one liquid computer implementing a computation (developing current flow and/or chemical gradient) while another liquid computer (a droplet) extracts the results of the computation. The motion of droplets of one liquid in another liquid is determined by thermal and chemical gradients, and directed by flows outside and inside the droplet [63–68]. If the gradients represent the solution of a computational problem then droplets travelling along the gradients might be seen as solving the problem. Such an experimental prototype of a droplet traversing a pH gradient is presented in [52]. There, a polydimethylsiloxane maze is filled with a solution of potassium hydroxide. An agarose block soaked in hydrochloric acid is placed at the destination site. A pH gradient establishes in the maze. Then a droplet of a mixture of mineral oil or dichloromethane with 2-hexyldecanoic acid is placed at the start site. The droplet travels along the steepest gradient of the potassium hydroxide. The steepest gradient is along the shortest path. Therefore, the droplet travels from its start site to the destination site along the shortest path [52].

The exact mechanics of the droplet motion are explained in [52] as follows. Potassium hydroxide, which fills the maze, is a deprotonating agent. The gradient of the protonated acid determines a gradient of the surface tension. The surface tension decreases towards the destination site. A

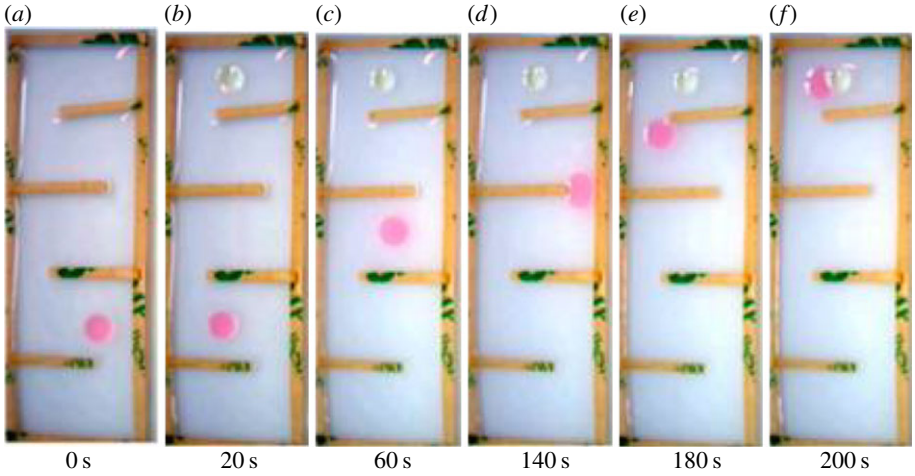

Figure 4. A decanol droplet (containing Oil Red O for colour) solves a maze. Adapted from [51] with kind permission of Jitka Čejková. (*a*) 0 s, (*b*) 20 s, (*c*) 60 s, (*d*) 140 s, (*e*) 180 s and (*f*) 200 s. (Online version in colour.)

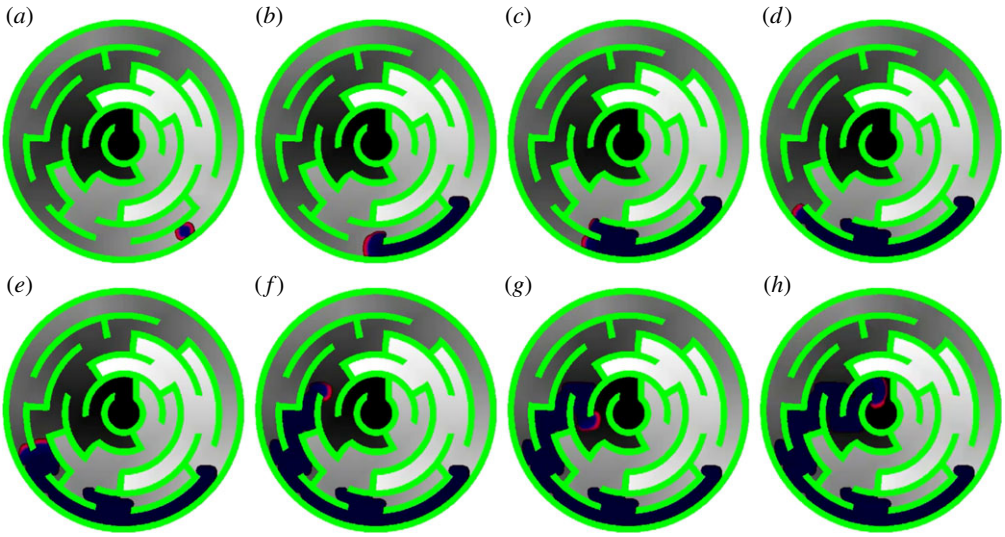

Figure 5. (*a–h*) Simulation of maze solving by slime mould using diffusion equations for attractants and Oregonator wave propagation for the slime mould. Concentration of diffusing attractants is shown by levels of grey. Active zone of slime mould is shown by red. (Online version in colour.)

flow of liquid—the Marangoni flow—is established from the site of the low surface tension to the site of the high surface tension. The droplet is moved by the flow [52].

Another prototype chemotactic droplet maze solver was demonstrated in [51]. The maze is filled with a solution of sodium decanoate in water. The sodium chloride diffuses from its host nitrobenzene droplet at the destination site. A gradient of the saline concentration is established. The gradient is steepest along the shortest path leading from any site in the maze to the destination. A decanol droplet moves along the steepest gradient till it reaches the droplet at the destination site (figure 4).

The experimental prototypes of travelling droplets laid the foundation of an emergent field of liquid robots [69,70]. There, droplets are studied as adaptive actuating and/or propulsive devices capable of navigation in dynamically changing environments.

The droplets tracing gradients behave in a manner similar to the slime mould *Physarum polycephalum*, though without permanent marking of the path selected. A *Physarum* maze solver, proposed in [71], is based on attraction of the slime mould to volatiles emitted by bacteria colonizing a virgin oat flake. Thus, to solve a maze, we place an oat flake in the maze's central chamber, and inoculate the slime mould into a peripheral channel. Chemoattractants from the oat flake diffuse along the maze's channels (figure 5*a*). The *Physarum* explores its vicinity by branching out protoplasmic tubes into openings of nearby channels (figure 5*b–e*). When a wavefront of diffusing attractants reaches the *Physarum*, the *Physarum* halts lateral exploration and develops an active growing zone propagating along the gradient of the attractants' diffusion (figure 5*f–h*). The thickest tube represents the shortest path between the sources of nutrients. Not only sources of nutrients can be placed at the destination site but also non-nutritional yet aromatic substances, e.g. roots of the medicinal plant *Valeriana officinalis* [72].

6. Fluidic logic

The first work on using fluids to implement logic gates can be traced back to the late 1950s/early 1960s [73–75]. The truth value of a variable was represented by high and low pressure in inlets and outlets and a computation was realized via interaction of fluid jet streams at junctions of the inlets. The basic principles of the fluidic devices are the laminar flow of a fluid, a jet interaction, a wall attachment and a vortex effect. The jet interaction is the phenomenon that occurs when fluid flows are arranged so that small opposing jets

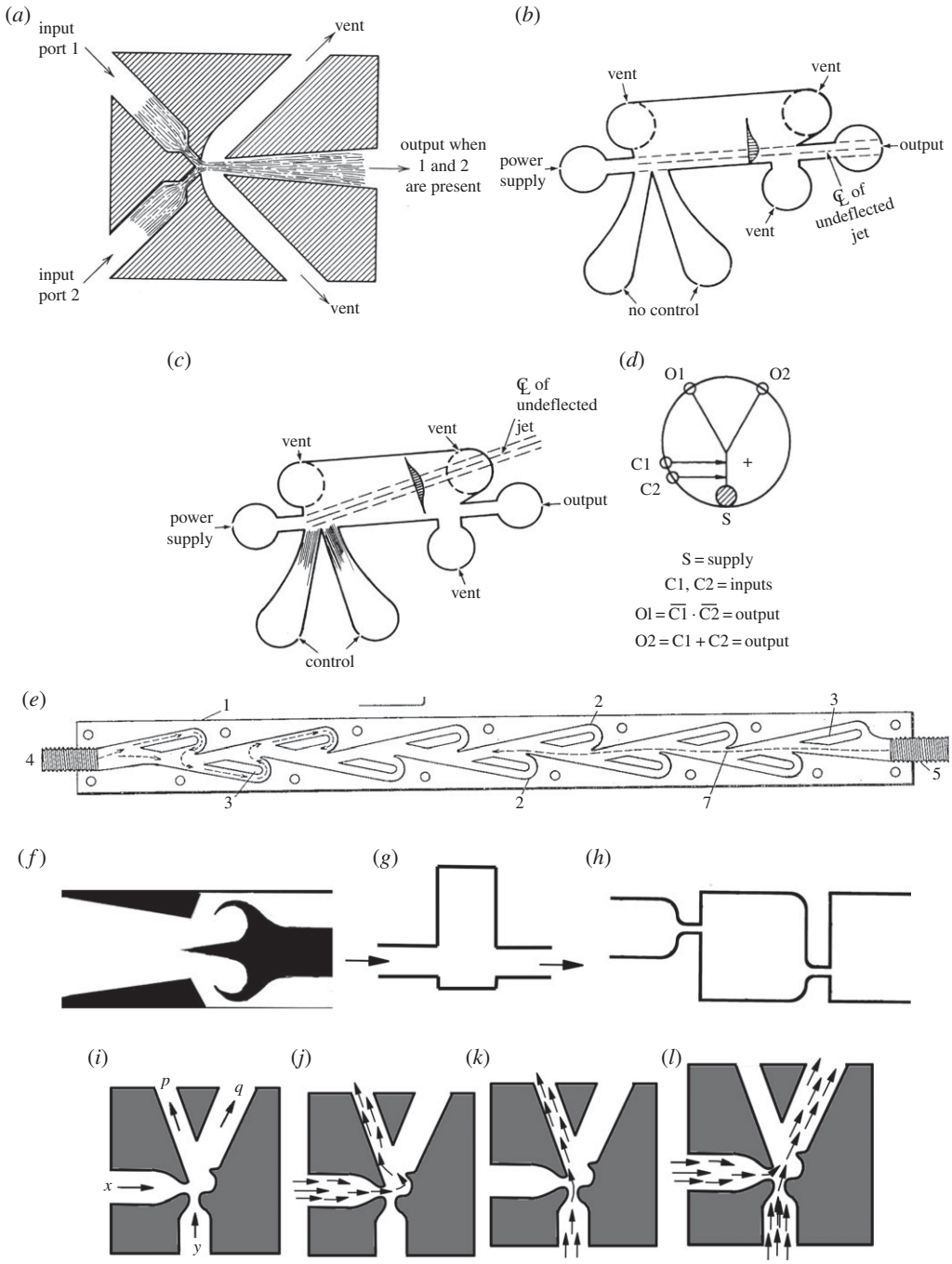

Figure 6. (*a*) Fluidic AND–NOT gate [36,76]. (*b,c*) Fluidic deflection type NOR element. From [74]: (*b*) undeflected jet, (*c*) jet deflected by control stream; ℄, contour line. (*d*) A diagram of the monostable fluid NOR–OR amplifier [77]. (*e*) Tesla diode [31]. (*f*) Scroll diode [35,74]. (*g*) Basic delay. Adapted from [33]. (*h*) Delay and diode. Adapted from [32]. (*i–l*) Hobbs gate: a hook-type fluidic half-adder. (*i*) Structure of the gate. (*j,k,l*) Dynamics of the fluid streams for inputs (*j*) $x = 1$ and $y = 0$, (*k*) $x = 0$ and $y = 1$, (*l*) $x = 1$ and $y = 1$. Modified from [34].

experience changes of direction which can be used as output signals. The wall attachment phenomenon is that the fluid attaches to a surface within a device and continues to flow over the surface until disturbed. The first devices, designed and fabricated in the 1960s, included beam deflection, turbulence, vortex and wall attachment amplifiers, AND, NOT, OR and XOR logic elements, counters and shift registers. The fluidic devices have been used in jet sensing, programmable sequence control, flameproof equipment, machine tool control, systems operating nuclear reactor coolant, servo-control in marine applications, missile and aircraft control, artificial heart-pumps, and lung ventilators [73–75].

The AND–NOT gate (figure 6*a*) is the most well-known device in fluidics, on, a par with the bistable amplifier. Two nozzles are placed at right angles to each other. When there are jet flows in both nozzles they collide and merge into a single jet entering the central outlet. If the jet flow is present only in one of the input nozzles it goes into the vent opposite. The horizontal output channel implements x AND y and later channels x AND NOT y and NOT x AND y.

A monostable beam deflection device comprises a power supply, controls/inputs and vents (figure 6*b,c*). When no inputs are present the fluid jet from the power source exits through the output (figure 6*b*). When one or both input jets are present, the jet from the power source is deflected into the vent and discharged (figure 6*c*) [74]. The fluid jet exits the output only if no input jet is present. This defines a NOR operation.

The monostable beam deflection device (figure 6*b*,*c*) can be transformed into a NOR–OR gate (figure 6*d*) by adding an output outlet instead of the vent [77]. When no control jets are present the jet from the power source exits via the outlet O1. If one or both signal jets are present, the jet from the power source is deflected into the outlet O2.

A fluidic diode is a two-terminal device that restricts, or even cancels, flow in one direction (backward direction). The Tesla diode [31] (figure 6*e*) and scroll diode [35,74] (figure 6*f*) are the most-known fluidic diodes (as well as the vortex diode, which is not discussed here).

The Tesla diode (figure 6*e*), called the 'valvular conduit' by its inventor [31], is composed of buckets and partitions arranged in such a manner that the forward flow propagates mainly along the axis (4–5 in figure 6*e*). In the backward direction (5–4 in figure 6*e*), fluid enters the branches and loops around to oppose the main flow.

In the fluidic scroll diode (figure 6*f*), the channel, or nozzle, converges in the backward direction and enters an annular cap. In the forward direction, the fluid flows through the throat and into a diffuser section. In the backward direction, the fluid enters the cap and is directed back towards an incoming flow, causing turbulence. A delay in the fluidic systems is implemented as a volumetric tank (figure 6*g*) with input and output pipes [33]. A step change in the input pressure appears as a similar change in the output pressure after a delay. The delay is caused by the turbulence. The amount of the delay is determined by the volume of the tank [33]. Another version of a delay element (figure 6*h*) combines orifices and volumes to have a low impedance in one direction of the flow.

A fluidic one-bit half-adder can be implemented on the basis of the gate proposed by Hobbs in 1963 [34] (figure 6*i*). Logical values are encoded into the presence of streams in the specified channels. When only input is TRUE, $x = 1$, a power jet stream enters the gate via channel x. The stream is turned by the hook and follows the channel p (figure 6*j*). When only input $y = 1$ the power jet stream entering the gate via channel y locks on (gets attached to) the left boundary wall of its channel, and propagates along the channel p (figure 6*k*). If both inputs are TRUE, streams entering x and y merge and follow the channel q (figure 6*l*). Thus, the stream exiting the channel p represents $p = x \oplus y$ and the stream exiting the channel q represents $q = xy$. The fluidic AND–NOT gate [36,76] had an unexpected 'reincarnation' in the logic gates implemented with swarms of soldier crabs [78–80] and plant roots [81,82]. In the crab gate, Boolean values TRUE and FALSE are encoded into the presence and absence of a swarm of soldier crabs in input or output channels (figure 7*a*). If a swarm is installed only in one of the input channels, it propagates along its original trajectory into the corresponding output channel, with minor dissipation of crabs into other channels. When both input channels have swarms of crabs, the crabs from different swarms collide at the junction. They change their velocity such that over 70–80% of crabs enter the central output channel (figure 7*c*). Thus, statistically, the central output channel represents function xy and lateral channels functions $\bar{x}y$ and $x\bar{y}$. The plant roots gate (figure 7*b*) proposed in [82] was an attempt to employ swarming behaviour of plant roots [84] in the implementation of logical functions. That is, roots propagating in the channels follow their original trajectories unless they encounter roots propagating in the other direction. When two swarms of propagating roots 'collide' their velocity changes towards a vector averaged over all swarm elements. Thus, if plant roots are present in both input channels they propagate into a central output channel xy.

7. Digital microfluidic logic

In fluidic logic devices, fluid jets are programmed by the geometry of channels and perform computation by interacting with each other. Boolean values are represented by pressure of the jets in the output channel. In digital microfluidics, signals are represented by droplets or bubbles travelling in the channel [47,48,50,53]. The droplets/bubbles also control pressure in the channels, thus affecting trajectories of other droplets/bubbles. An example of a fluidic gate, designed in [47], with two inputs x and y and two outputs is shown in figure 8*a*–*d*. An oil droplet is introduced into an aqueous phase. When the droplet enters the channel with the larger flow rate, the pressure drop increases across the channel containing two-phase emulsions, particularly at a low capillary number.

Cheow *et al.* [47] designed a ratio of tubes and flows (figure 8*a*) such that the following phenomena take place. If the flow through A to C exceeds the flow through A; the regime is laminar; therefore all flow from x goes via AC. An oil droplet entering A travels into C (figure 8*b*). The flow through the bridge between A and B exceeds half of the flow through B. Thus, an oil droplet entering B also travels into C (figure 8*c*). When a droplet from A enters channel C the hydrodynamic resistance of A increases. The flow via the bridge connecting A and B becomes less than half of the flow through B. The droplet entering B travels into channel D (figure 8*d*).

Using similar principles, Morgan *et al.* [85] implemented a one-bit half-adder. When only one of the input channels represents '1' the droplets from this channel go into channel S (figure 8*e*,*f*). When both inputs are '1' the droplets travel into lateral channels (figure 8*g*).

Other variants of fluidic gates are realized in [50] using surface tension-based passive pumping and fluidic resistance, and in [49].

8. Billiard-ball computing with droplets and marbles

In billiard-ball computing with droplets, the presence/absence of a droplet in a given time or space symbolizes TRUE/FALSE. The droplets compute when they collide with each other and change their velocity vectors as a result of the collision.

Most logic gates implemented in fluidic devices (§6) use the phenomenon of merging colliding jet streams (figure 6*a*) and excitation wave-fragments (figure 11*g*). Thus, input jet streams or wave-fragments x and y propagating, beyond the collision site, along their original trajectories represent functions $x\bar{y}$ and $\bar{x}y$. A stream or a wave-fragment propagating along a new trajectory represents the function xy. Discrete soft and liquid bodies do not always merge when they collide but often are reflected. Thus, they can implement collision-based gates.

Collision-based computation, emerging from Fredkin–Toffoli conservative logic [86], employs mobile compact finite patterns, which implement computation while

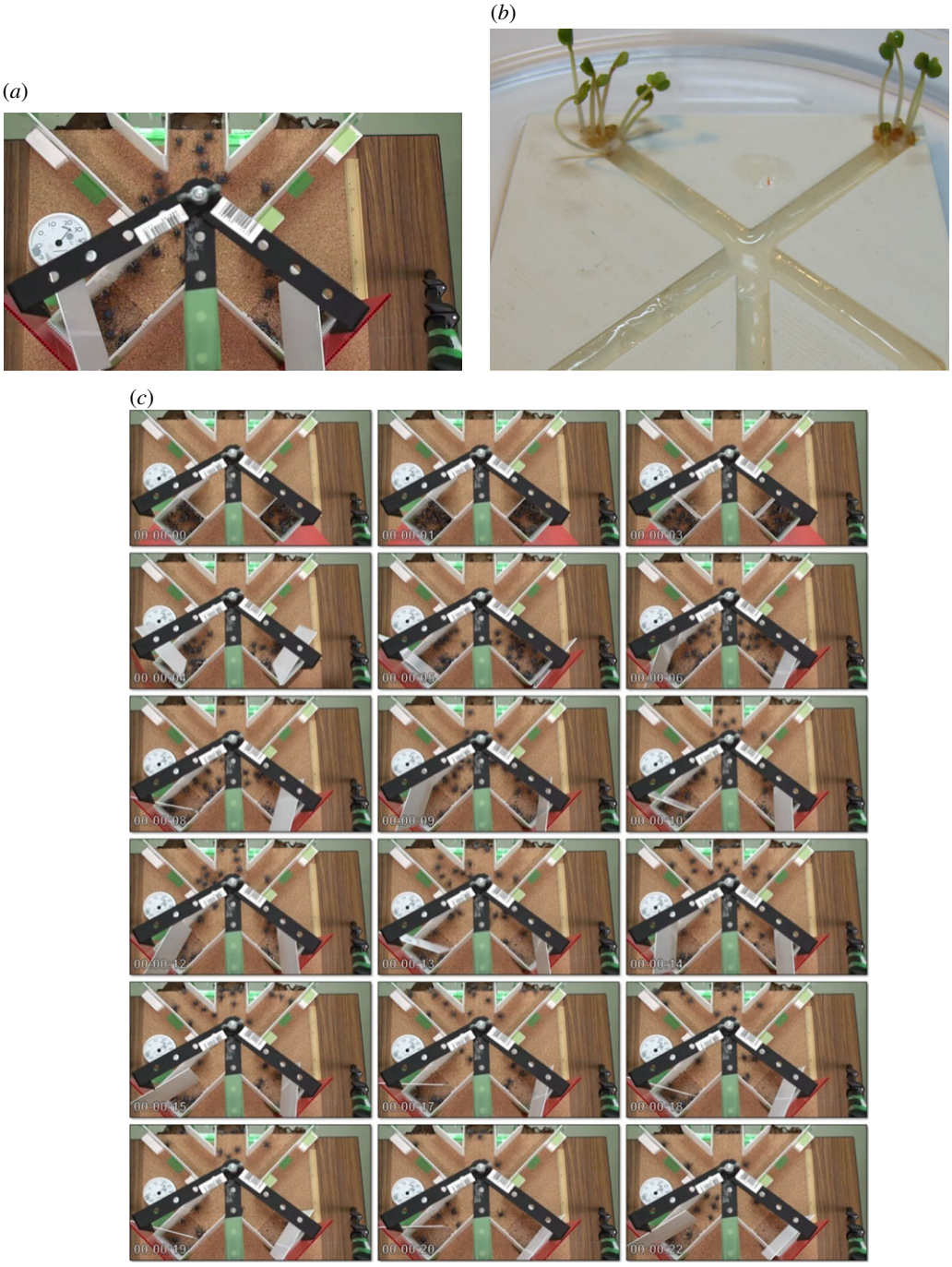

Figure 7. (*a*) A snapshot of the experimental set-up of AND–NOT gate implemented with soldier crabs. From [83] with kind permission of Yuta Nishiyama and Yukio Gunji. The crabs are placed in one or two input channels, shown at the bottom of the photos, and persuaded to move towards three output channels, shown at the top of the photos. (*b*) Experimental set-up of plant root gate. (*c*) Snapshots of operating crab gate for inputs 11: both input channels have swarms of crabs. See video at https://vimeo.com/242345427. (Online version in colour.)

interacting with each other [87]. Information values (e.g. truth values of logic variables) are given either by the absence or the presence of the localizations or by other parameters of the localizations. These localizations travel in space and perform computation when they collide with each other. Thus, the localizations undergo transformations: they change velocities, form bound states and annihilate or fuse when they interact with other localizations. Information values of localizations are transformed as a result of collision and thus a computation is implemented.

When two hard balls collide they are reflected in such a manner that the trajectory of a reflected ball is at an angle of less than 180° to the trajectory of the same ball not involved in the collision (figure 9*a*). If the presence of balls represents TRUE values of Boolean variables x and y, then the trajectories of the reflected balls represent $\bar{x}y$ and $x\bar{y}$. This was the inspiration for the Fredkin gate [86]. When balls are soft they are compressed on impact and propagate for some period of time as conjunct bodies. Then their shapes are restored and they bounce back; thus their output trajectories are shifted in time–space (figure 9*b*). When soft bodies impact each other under particular regimes they might merge into a single ball and lose their momentum (figure 9*c*); in this case, we have only three output trajectories instead of four. The gate shown in figure 9*c* is a fusion gate analogous to figure 6*a*.

Outcomes of the collisions between liquid droplets depend on the relationship between fluid inertia and tension

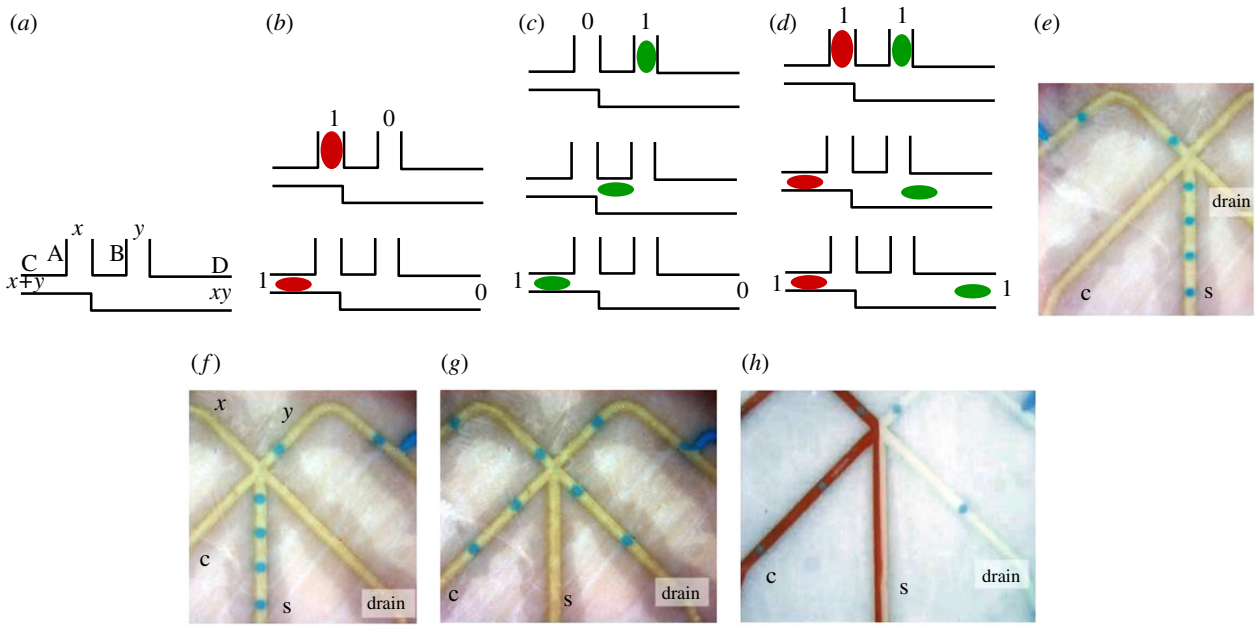

Figure 8. (*a–d*) Microfluidic gate OR–AND, redrawn from [47]; oil droplets are coloured red and green for distinction only. Vertical channels are inputs, horizontal channels are outputs. (*e–h*) Snapshots of experimental implementation of microfluidic half-adder by Morgan *et al.* [85]: (*e*) $x = 1$, $y = 0$, (*f*) $x = 0$, $y = 1$, (*g*) $x = 1$, $y = 1$, (*h*) oil entering channel x is coloured to demonstrate a deflection of flow. Adapted from [85]. (Online version in colour.)

(Weber number) of the colliding droplets and their offset. Binary collisions between droplets have been analysed exhaustively by Ashgriz & Poo in 1990 [89] and 20 years later by Rabe *et al.* [88]. Based on their results, we can derive the following experimental droplet gates: stretching separation (figure 9*d*) and reflexive separation (figure 9*f*) of colliding droplets represent a soft balls gate; coalescence of droplets (figure 9*e*) represents a fusion gate (figures 9*c* and 6*a*). For certain parameters of the droplet collisions, one or more stationary droplets are formed [89] (figure 9*g*); they could represent results of the AND gate and even be used as elementary memory units (the presence of a stationary droplet is '1' and the absence is '0').

Mertaniemi *et al.* [53] explicitly interpreted collisions between droplets on a hydrophobic surface in terms of Boolean logic gates. They programmed trajectories of droplets, and thus architectures of the logic gates, by the geometry of grooves, on the hydrophobic surface, along which the droplets travel. Examples of two gates are the NOT gate (figure 9*h–j*) and the OR–AND gate (figure 9*k–n*). In the NOT gate (figure 9*h*), there is a droplet travelling along the channel labelled '1'. When this droplet '1' collides with the droplet travelling along the channel x, the droplet '1' is reflected into the south-west channel x (figure 9*i*). When input x is FALSE and only the droplet in channel '1' is present, the droplet '1' travels into the channel $\bar{x}$. The OR–AND gate (figure 9*k*) shows several channels leaving the collision site, and thus that the droplets x or y are always routed to the channel $x + y$ when each of the droplets enters the gate alone (figure 9*l*,*m*). When both droplets enter the gate, they collide. Then one droplet enters the channel xy while the other droplet still travels to the channel $x + y$ (figure 9*n*).

Instead of running droplets on a hydrophobic surface, we can coat the droplets with a hydrophobic power. The droplets then become liquid marbles. The liquid marbles, proposed by Aussillous & Quéré in 2001 [90], are liquid droplets coated by hydrophobic particles at the liquid/air interface (figure 10*a–c*). In 2016, I proposed to make experimental laboratory prototypes of computing devices allowing the liquid marbles to explore additional degrees of freedom to travel in different directions [92]. The first collision-based logic gate with liquid marbles was prototyped by Draper *et al.* [54]. An example of the liquid marble gate in action is shown in figure 10*d*.

Computing schemes involving 'proper' collision-based gates require a synchronization of signals. Such synchronization is indeed achievable but places an additional burden on preparation of data for computation; thus, simultaneously with developments of synchronous circuits I considered producing experimental prototypes of asynchronous devices based on cantilever moving parts, actuated by liquid marbles [92].

In 1965, J. T. Godfrey [93] proposed a mechanical binary digital computer: the configuration of flip-flops arranged on an inclined surface and operated by metal balls rolling down the surface. The design inspired my group to prototype an asynchronous binary counter actuated by liquid marbles [90] (figure 10*e*). Droplet and liquid marble devices use the force of gravity to operate. This can be avoided by using self-propulsive liquid marbles, e.g. aqueous ethanol marbles on a water surface [94,95] or polypyrrole and carbon black marbles driven by light [96].

9. Reaction–diffusion computers

All living systems, from cells to brain cortex, display excitable dynamics as part of their dynamical patterns [97–99]. Creatures without a nervous system, e.g. plants [100–108], slime moulds [109–115] and fungi [116,117], employ excitation dynamics, manifested in calcium waves and action-potential-like spikes, in their decision-making processes. The electrical activity in plants, slime mould and fungi might be associated with calcium waves [111,118–125]. Decision-making with calcium waves propagating in living substrates strongly relates to the theory and practice of reaction–diffusion computing.

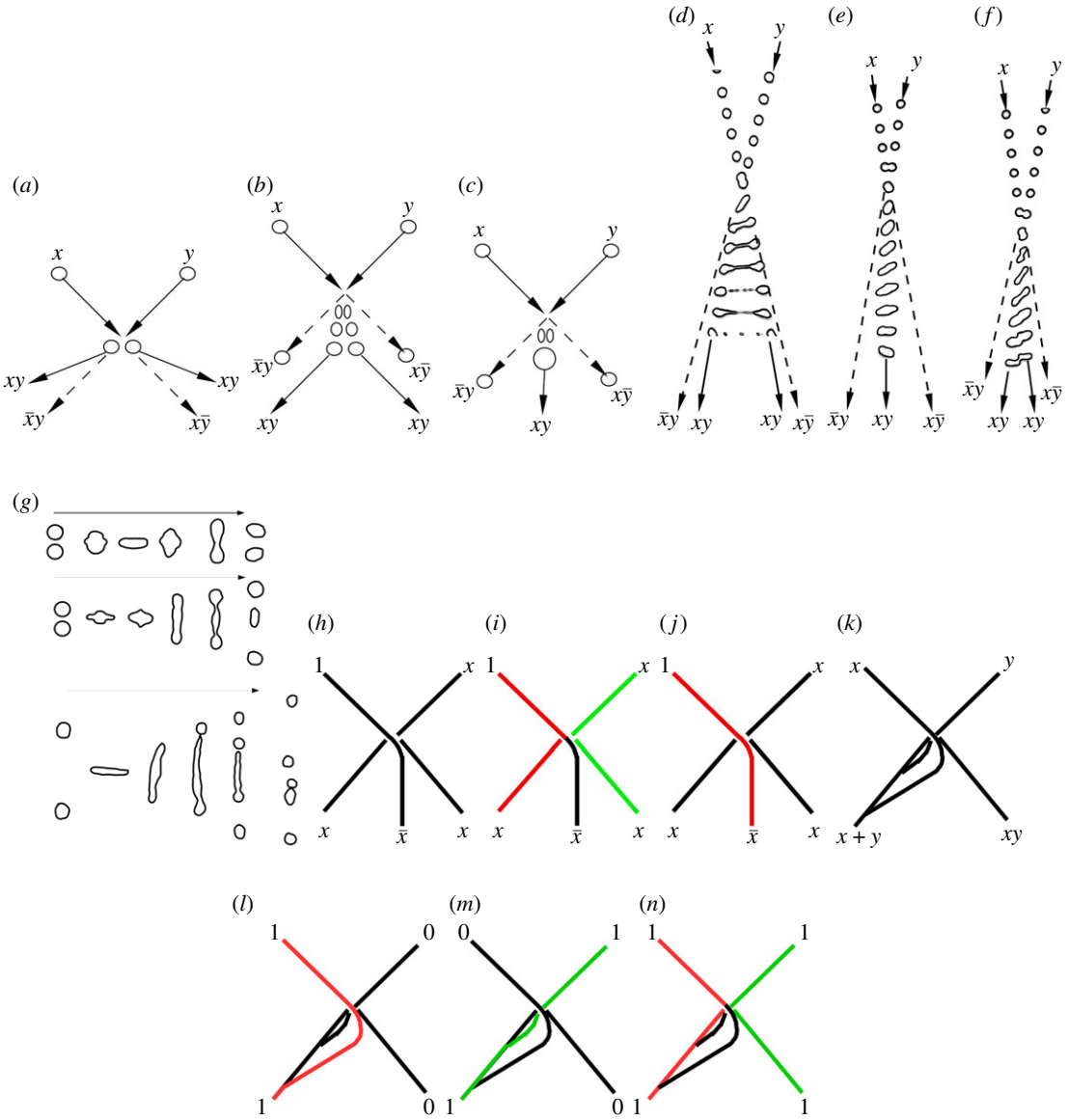

Figure 9. Collision-based computing with droplets and liquid marbles. (*a*) Hard balls gate, Fredkin gate. (*b*) Soft balls gate, Margolus gate. (*c*) Fusion/coalescence gate. (*d–f*) Gates derived from laboratory experiments [88] with droplets colliding with various offsets: (*d*) stretching separation, (*e*) coalescence and (*f*) reflexive separation. Illustrations of colliding droplets are redrawn from fig. 4 of [88]. (*g*) Outcome of binary droplet collision experimentally found by Ashgriz & Poo [89]; Weber numbers, from top to bottom are We = 23, We = 40 and We = 96. Collisions are redrawn from [89]. (*h–n*) Schemes of gates implemented with droplets on a hydrophobic surface in [53]. (*h–j*) NOT gate, scheme (*h*), $x = 1$ (*i*), $x = 0$ (*j*). (*k–n*) OR–AND gate, scheme (*k*), $x = 1$, $y = 0$ (*l*), $x = 0$, $y = 1$ (*m*), $x = 1$, $y = 1$ (*n*). In (*h–n*), the pathway of a droplet originated in channel *x* is coloured red, and in channel *y* green. (Online version in colour.)

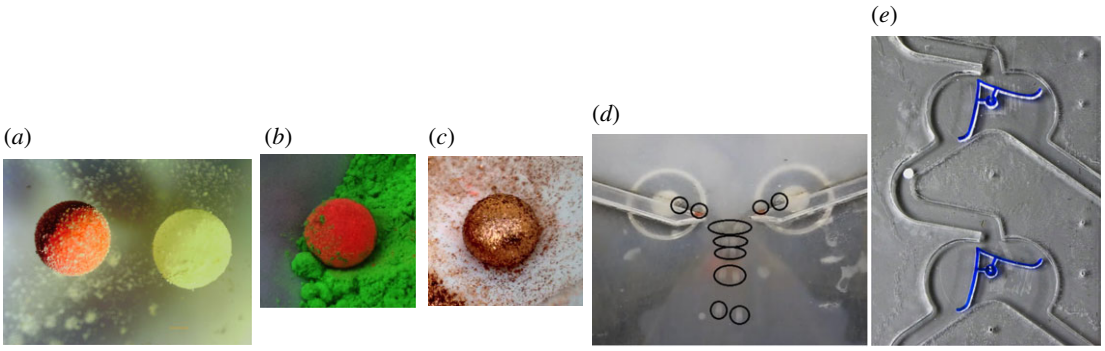

Figure 10. (*a*) Liquid marbles with *Lycopodium* coating and water cargo on the right and a mix of red Indian ink and water on the left; marbles are around 5 µl in volume. (*b*) Fifty microlitre water marble coated by red fluorescent fingerprint powder. (*c*) Fifty microlitre water marble coated by copper particles. (*c*) Soft balls gate, figure 9*b*, implemented with liquid marbles, filmed by a high-speed camera; the gate was prototyped by Draper *et al.* [54]. Adapted from [54]. (*d*) A fragment of the liquid marble binary counter presented in [91]. (Online version in colour.)

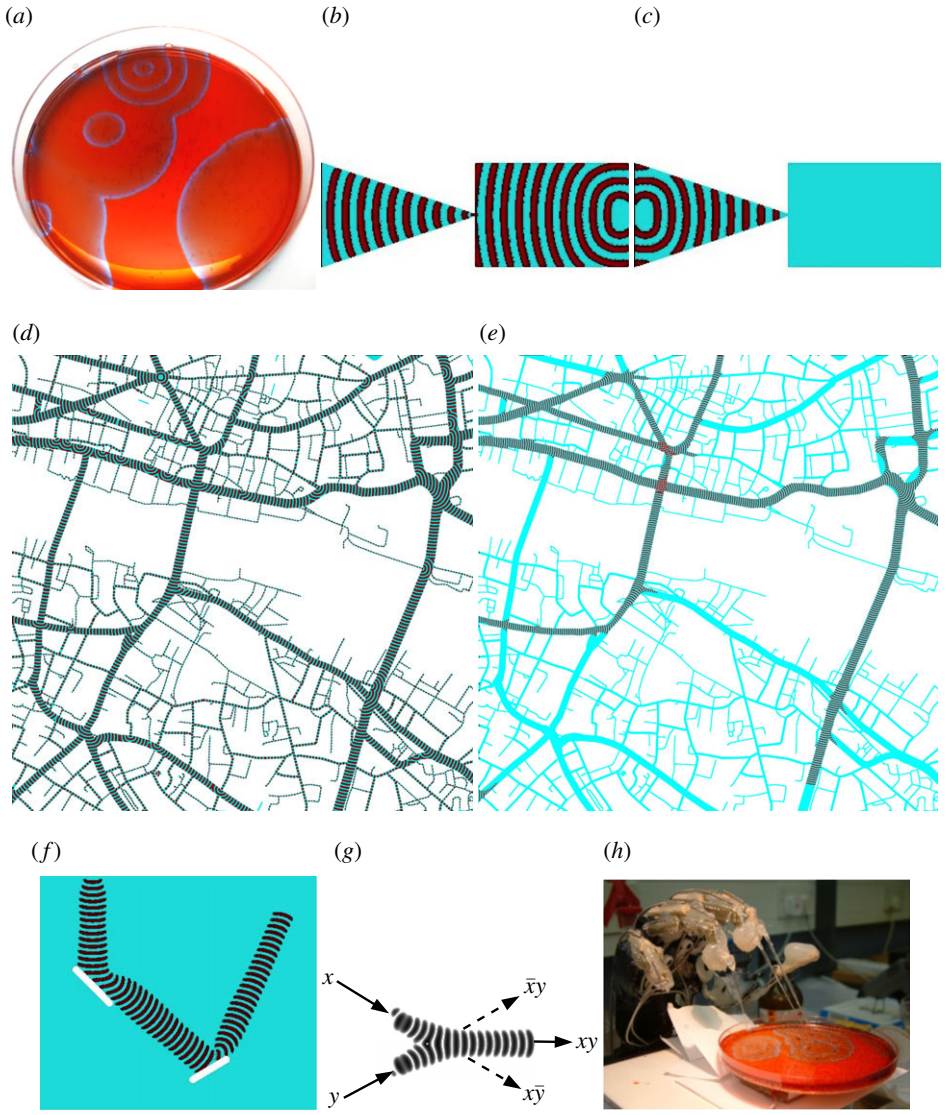

Figure 11. (*a*) A thin-layer BZ reaction; travelling oxidation wavefronts are blue. (*b,c*) Computer model of Agladze diode. (*b*) Forward propagation. Excitation wavefront propagates from the right to the left. (*c*) Backward propagation. Excitation wavefront propagates from the left to the right. (*d,e*) Exploration of London street networks with fully excitable (*d*) and sub-excitable (*e*) media. Time lapse snapshots two-variable Oregonator model. (*f*) Routing of a wave-fragment in a sub-excitable medium. The medium is sub-excitable but two rectangular shapes (white rectangles) are not excitable. Grid size is 500×500 nodes. The pictures are not snapshots of many wave fronts generated at the initial stimulation point, but time lapsed snapshots of a single wave-fragment recorded every 150th step of numerical integration. (*g*) Collision-based gate. Case shown when both inputs have value TRUE; thus two wave-fragments collide. Time lapse overlays. One fragment is travelling from north-west to south-east, another fragment from south-west to north-east. The wave-fragments collide and fuse into a new localized excitation travelling east. (*h*) Robotic hand interacts with Belousov–Zhabotinsky medium. When the bending fingers touch the chemical medium, glass 'nails' fitted with capillary tubes release small quantities of colloidal silver into the solution and this triggers additional circular waves. Adapted from [131]. (Online version in colour.)

A reaction–diffusion computer [18,126,127] is a spatially extended chemical system that processes information by transforming an input concentration profile to an output concentration profile in a deterministic and controlled manner. In reaction–diffusion computers, the data are represented by concentration profiles of reagents, information is transferred by propagating diffusive and phase waves, computation is implemented via the interaction of these travelling patterns (diffusive and excitation waves), and results of the computation are recorded as a final concentration profile. Chemical reaction–diffusion computing is among the leaders in providing experimental prototypes in the fields of unconventional and nature-inspired computing.

The Belousov–Zhabotinsky (BZ) reaction—periodic oxidation of malonic acid in solution [128–130], has been a key substrate for implementing reaction–diffusion computers for nearly the last 40 years. In these computing devices, information is represented by travelling oxidation wave fronts (figure 11*a*) and the computation is programmed by geometrical constraining of the medium or configurations of the excitation initiation sites.

Research on BZ-based information processing started in the mid-1980s when Kuhnert, Agladze & Krinsky demonstrated that a thin layer of light-sensitive BZ reaction can implement contrast modification, detection of a contour and smoothing of the half-tone images projected onto the medium [39,132]. These results ignited an almost 40 year epoch of information processing with BZ medium. Work on image processing with BZ continued till the early 2000s [133–137].

In the mid-1990s, the Showalter laboratory produced a series of experimental prototypes of logic gates implemented

via interaction of oxidation wavefronts in geometrically constrained BZ medium [40]. Following this, numerous devices were modelled and/or implemented in the experimental laboratory, including signal switches [138], counters [38], a one-bit adder [139], a many-bit binary adder [140] and decoder [141], three-valued logic gates [142] and a device for square root approximation [143].

Design of potential computing circuits was facilitated by the discovery of a chemical diode [37]. The diode is made of two plates covered with excitable solution. The corner of one plate is close to the plane side of the other plate. An excitation wavefront travelling in the forward direction reaches the contact site between the plates as a planar wave, it propagates through the contact site and then continues expanding in the triangular part of the device (figure 11*b*). The wave-fragment travelling in the backward direction slows down while propagating towards the corner of the triangular plate (figure 11*c*). At the contact point, the size of the wave-fragment becomes so small, for the level of the medium's excitability, that it is annihilated without crossing the contact site between the plates.

The above prototypes constrained BZ medium in templates, that is, BZ computers were programmed by architecture. There is another option to realize logic gates using BZ. This is a collision-based, or dynamical, computation [86,87]; see §8. In 2001, Sendiña-Nadal *et al.* [144] experimentally demonstrated the existence of localized excitations—travelling wave-fragments that behave like quasi-particles in the photosensitive sub-excitable BZ medium. In the early 2000s, I proposed that the compact wave-fragments can represent Boolean values and execute logic gates by colliding with each other [145]. The wave-fragments can be routed in the medium by using non-excitable domains as reflectors (figure 11*f*). I employed the localizations to construct several logic gates and circuits [145–149].

BZ medium is also used for optimization tasks, e.g. to assist in maze solving [150–152] and to calculate the shortest collision-free path [87]. Recently, my group found that by tuning the excitability of the medium we can select the critical features of street networks [153,154]. In excitable BZ, oxidation wavefronts traverse all streets of the network (figure 11*d*). A pruning strategy is adopted by the medium with decreasing excitability when wider and ballistically appropriate streets are selected (figure 11*e*).

In the early 2000s, the first-ever excitable chemical controller mounted on-board a wheeled robot was constructed and tested under experimental laboratory conditions [20,45,87], and also a robotic hand was interfaced and controlled using BZ medium [128] (figure 11*h*). Litschel *et al.* [155] showed that by linking micro-reactors with BZ and establishing excitation and inhibitory connections between the neighbouring reactors, it is possible to generate travelling patterns of oscillatory activity resembling the neural locomotive patterns.

Control of a robot with oxidation wavefronts can be embedded directly in the actuating materials. This can be done by impregnating a pH-sensitive gel with a catalyst and immersing it in the catalyst-free BZ solution: a peristaltic motion will be observed [156]. Such an approach can be advanced to other types of smart materials and soft robots [157,158].

The collision-based gate shown in figure 11*g* can be also implemented in a geometrically constrained medium, where wave-fragments interact at the junctions of the excitable channels (figure 12) [159]. In excitable mode, stimulation of a single (figure 12*b*, input *x*) input leads to wavefronts propagating to all channels. In sub-excitable mode, a wave-fragment from the input channel propagates ballistically to an output channel (figure 12*c*), but when both input channels are excited the wave-fragments fuse and propagate into the central vertical channel (figure 12*e*). The fusion gates can be cascaded into a one-bit half-adder (figure 12*f–i*), and further to a many-bit full adder [159] and Fredkin and Toffoli logically reversible gates [161].

Fine-grained compartmentalization of BZ solutions can be achieved by preparing emulsions or liquid droplets of BZ solution in an oil and liposomes [162–168]. Then each of the droplets can be seen as a computing element interacting with its neighbours via reagents diffusing in oil. Information transmission, as presented by excitation wave fronts, between BZ droplets [164,165,169] has been demonstrated in laboratory experiments. Experimental laboratory computing devices made from arrays of BZ droplets or vesicles are the memory devices made from BZ–oil emulsion [170] and the NOR gate made from BZ droplets with inhibitory coupling [171]. Recently, my group demonstrated prototypes of BZ liquid marbles, BZ solution coated with a hydrophobic powder [172]. There is evidence of oxidation wavefront transmission between BZ liquid marbles, possibly via the gaseous phase; however, more experimental evidence is required to establish the design of potential computing architectures.

As demonstrated in computer experiments, by arranging a configuration of BZ droplets and by tuning sizes of pores between BZ vesicles, it is possible to implement Boolean gates, including collision-based polymorphic gates [173] and binary arithmetic circuits [160,174–176]. In the example shown in figure 12*j*, a one-bit half-adder is implemented in a simulated ensemble of two-dimensional BZ vesicles. The outputs from the XOR operation are recombined with an OR operation with additional discs in the top right. The circuit employs three methods of signal modulation: connection angle, disc size and aperture efficiency. Vesicles sizes and diameters of pores between vesicles are selected intentionally to perform the desired operations. The half-adder implemented in uniformly sized vesicles having the same diameters of pores is shown in figure 12*k*.

Recently, Gorecki *et al.* [177] demonstrated how to make a frequency of oscillation-based OR gate and one-bit memory in an array of coupled oscillatory BZ droplets and to evolve a classifier of BZ droplets [178].

BZ reaction is not the only chemical medium for unconventional computing. In the mid-1990s, Tolmachiov & Adamatzky developed prototypes of reaction–diffusion computing devices capable of approximation of the Voronoi diagram of a planar point set [44] and calculation of a skeleton of a planar shape [43]. Several experimental laboratory prototypes of precipitating processors have been built for implementation of an XOR gate [179], and computation of a skeleton of a planar shape [179] and Voronoi diagrams [180].

10. Discussion

Several contributions to this special issue have demonstrate that a creature does not need a nervous system, in its classical sense, to fuse sensorial inputs, process information and make a decision. The most exciting examples include learning by

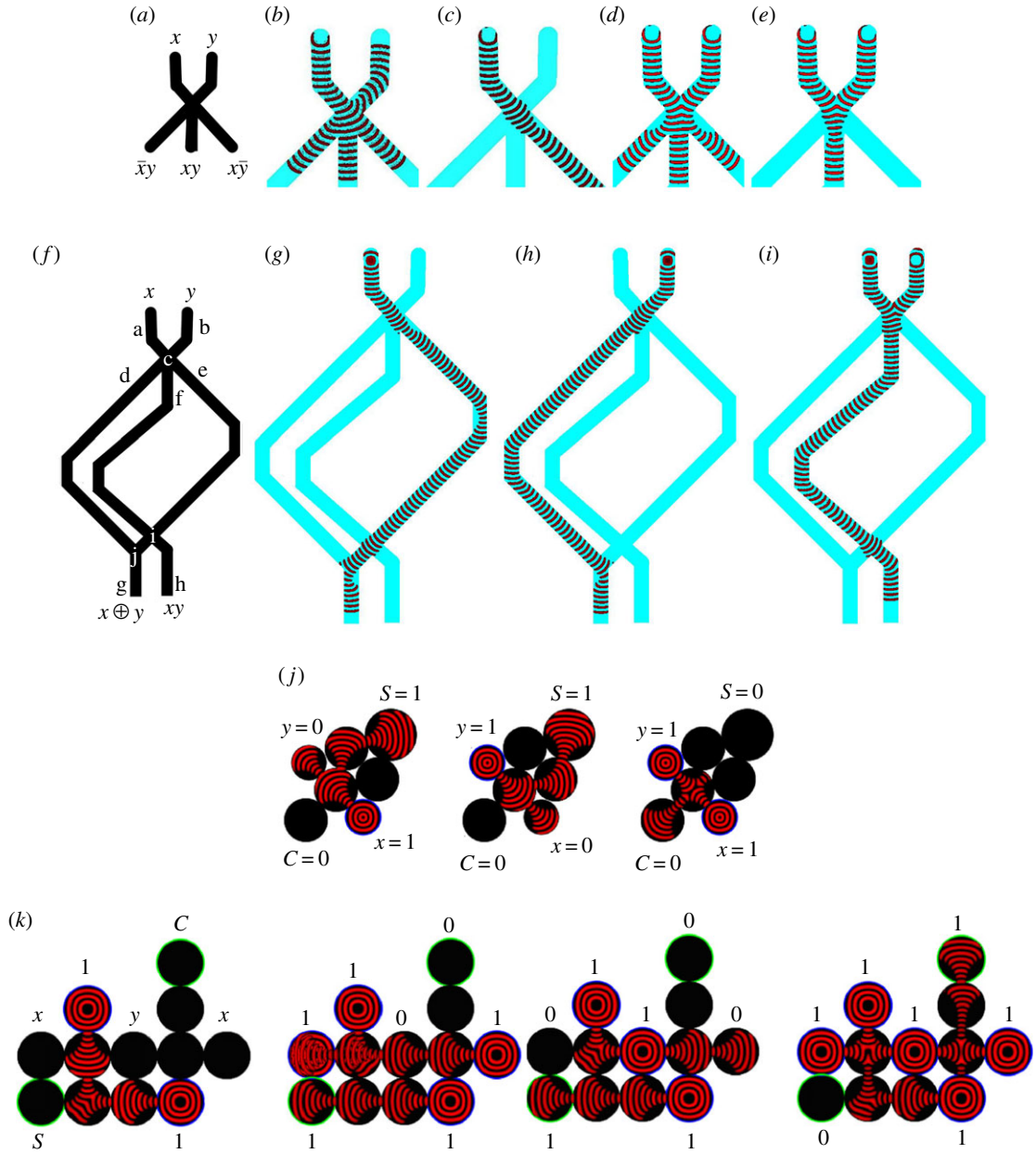

Figure 12. (*a–e*) Fusion gate. (*a*) Scheme: inputs are *x* and *y*, outputs are *xy*, $\bar{x}y$, $x\bar{y}$. (*b–e*) Time lapse overlays of excitation waves. (*b*) Excitable mode, $x = 1$, $y = 0$. (*c*) Sub-excitable mode, $x = 1$, $y = 0$. (*d*) Excitable mode, $x = 1$, $y = 1$. (*e*) Sub-excitable mode, $x = 1$, $y = 1$. (*f*) A scheme of a one-bit half-adder: input channels are a and b, output channels are g and h, internal channels are d, e, f, and junctions are c, i and j. Input variables *x* and *y* are fed into channels a and b, results $x \oplus y$ and *xy* are read from channels g and h. (*g–i*) Time lapse overlays of excitation waves propagating in the one-bit half-adder for inputs (*g*) $x = 1$, $y = 0$, (*h*) $x = 1$, $y = 0$, (*i*) $x = 1$, $y = 1$. Sites of initial segment-wise perturbation are visible as discs. Grid size is 500×790 nodes. See details in [159]. (*j*) Composite half-adder implemented in two-dimensional BZ vesicles: $S = x \oplus y$, $C = x \cdot y$, where inputs and outputs are all connected to a central reactor disc which can achieve both the AND and XOR functions. Adapted from [160]. (*k*) Half-adder made from uniform BZ vesicles. Adapted from [160]. (Online version in colour.)

the slime mould, morphogenetic positional computing, distributed information processing in plant organs, and neuronal-like activity of bacterial biofilms. In the present paper, I show that a substrate does not need to be alive or posses any particular electrical or biochemical properties to compute: even a liquid, which you would be unable to keep in your hands, can perform sophisticated computing circuits.

Back in 2007, while at the 'Unconventional Computation: Quo Vadis?' conference in Santa Fe I met Norman Margolus (famous for his block cellular automata model of billiard-ball computers, co-design of the Cellular Automata Machine, and Margolus–Levitin theorem [181]). During our discussion about the nature of computation, Norman stated that 'any object/substrate either does not compute or is a universal computer'. Fully agreeing with this statement, I would like to highlight that the time for theorizing that 'natural systems' compute is over. It is time to produce working laboratory prototypes of actual computing devices based on unconventional computing substrates. This is why in this paper I have exhibited a kaleidoscope of the working prototypes of liquid-based computing devices. I have shown that one can implement logic gates using interacting stream jets, colliding liquid droplets and marbles, and excitation wavefronts in nonlinear chemical medium. Most of the prototypes demonstrated are not liquid-specific. For example, gradient tracing by liquid droplets can be imitated by slime mould growing along a gradient of chemoattractants, and logic gates implemented by jet streams can be equally realized via collision between swarms of soldier crabs or growing plant roots.

The future potential of liquid-based computing is enormous. By selecting an appropriate cargo in liquid marbles, we can implement chemical reactions with two marbles. Thus information values carried by the marbles will not be just the binary physical presence of a marble at a given time in a given space but also concentrations of chemical species inside input and output marbles. A droplet or a marble filled with Belousov–Zhabotinsky (BZ) reaction medium can perform massive-parallel computation by itself because there are thousands of chemical micro-reactors that may act as elementary processors. At the same time, several BZ marbles can implement billiard-ball computing when rolling under gravity in a geometrically constrained space.

In this brief review, I have touched on all principal developments in liquid computing but liquid electronics. The breadth and depth of the liquid electronics 'eco-system' would require a separate review paper. Example 'species' of liquid electronics devices are liquid–solid phase reversible change of conductivity controlled by temperature [182], field-controlled electrical switch [183], liquid field effect transistor [184] and optical liquid droplet switch [185]. There is a also a huge, and largely unexplored, potential in combining mechanical properties of the liquid jets, droplets and marbles with electrical and optical properties of their solvents and solutes. All these provide scope for future studies.

The primary disadvantages of fluidic computers are now, as they were in the 1960s, lower operating speed (unless air jets are employed), higher power loss and entrapped air [186]. These problems become less important when considered in the context of reconfigurable bioinspired robots or control systems where speed is not critical.

What are the advantages of liquid computers? They do not need an electricity or any other artificial power source and can work just under gravity. This makes liquid computers invincible to electro-magnetic fields and fault tolerant (this is why some components from fluidic logic devices from the 1960s are still used in nuclear reactor control systems [187–189] and fighter jets [190–192]). In many prototypes of fluid computers, there are no moving parts (apart from fluid); therefore the devices have a lifetime substantially longer than mechanical or electrical computers. Fluidic devices can be integrated with and embedded in sensing and actuating materials; therefore they are impeccable controllers for soft-bodied robots [193]. The advantage of liquid droplets and marbles is the ease of their generation and manipulation; this is already well demonstrated by digital microfluidics applications [194–196].

Competing interests. The author declares that he has no competing interests.

Funding. No funding has been received for this article.

Endnotes

[1]Analyses of fluid-like behaviour of ants was inspired by early results on fluid-like behaviour of crowds [14–16].
[2]Tesla diode was proposed in 1920s but in relation to computation [31].
[3]The hydraulic equation solvers are discussed in the context of electrical and mechanical solvers in [25].

References

1. Alim K, Amselem G, Peaudecerf F, Brenner MP, Pringle A. 2013 Random network peristalsis in *Physarum polycephalum* organizes fluid flows across an individual. *Proc. Natl Acad. Sci. USA* **110**, 13 306–13 311. (doi:10.1073/pnas.1305049110)
2. Sato M, Wong TZ, Allen RD. 1983 Rheological properties of living cytoplasm: endoplasm of *Physarum* plasmodium. *J. Cell Biol.* **97**, 1089–1097. (doi:10.1083/jcb.97.4.1089)
3. Tero A, Yumiki K, Kobayashi R, Saigusa T, Nakagaki T. 2008 Flow-network adaptation in *Physarum* amoebae. *Theory Biosci.* **127**, 89–94. (doi:10.1007/s12064-008-0037-9)
4. Wohlfarth-Bottermann K. 1979 Oscillatory contraction activity in *Physarum*. *J. Exp. Biol.* **81**, 15–32.
5. Alim K, Andrew N, Pringle A, Brenner MP. 2017 Mechanism of signal propagation in *Physarum polycephalum*. *Proc. Natl Acad. Sci. USA* **114**, 5136–5141.
6. Alim K. 2018 Fluid flows shaping organism morphology. *Phil. Trans. R. Soc. B* **373**, 20170112. (doi:10.1098/rstb.2017.0112)
7. Boisseau RP, Vogel D, Dussutour A. 2016 Habituation in non-neural organisms: evidence from slime moulds. *Proc. R. Soc. B* **283**, 20160446. (doi:10.1098/rspb.2016.0446)
8. Dussutour A, Latty T, Beekman M, Simpson SJ. 2010 Amoeboid organism solves complex nutritional challenges. *Proc. Natl Acad. Sci. USA* **107**, 4607–4611. (doi:10.1073/pnas.0912198107)
9. Vallverdú J *et al.* 2018 Slime mould: the fundamental mechanisms of biological cognition. *Biosystems* **165**, 57–70. (doi:10.1016/j.biosystems.2017.12.011)
10. Whiting JG, Jones J, Bull L, Levin M, Adamatzky A. 2016 Towards a *Physarum* learning chip. *Sci. Rep.* **6**, 19 948. (doi:10.1038/srep19948)
11. Burd M, Archer D, Aranwela N, Stradling DJ. 2002 Traffic dynamics of the leaf-cutting ant, *Atta cephalotes*. *Am. Nat.* **159**, 283–293. (doi:10.1086/338541.)
12. Fourcassié V, Dussutour A, Deneubourg J-L. 2010 Ant traffic rules. *J. Exp. Biol.* **213**, 2357–2363. (doi:10.1242/jeb.031237)
13. Detrain C, Deneubourg J-L. 2006 Self-organized structures in a superorganism: do ants 'behave' like molecules? *Phys. Rev.* **3**, 162–187. (doi:10.1016/j.plrev.2006.07.001)
14. Helbing D. 1998 A fluid dynamic model for the movement of pedestrians. See http://arxiv.org/abs/9805213.
15. Henderson LF. 1974 On the fluid mechanics of human crowd motion. *Transp. Res.* **8**, 509–515. (doi:10.1016/0041-1647(74)90027-6)
16. Hughes RL. 2003 The flow of human crowds. *Annu. Rev. Fluid Mech.* **35**, 169–182. (doi:10.1146/annurev.fluid.35.101101.161136)
17. Adamatzky A. 1996 Reaction-diffusion computer: massively parallel chemical computation. In *Parcella 1996, Proc. VII Int. Workshop on Parallel Processing by Cellular Automata and Arrays, Berlin, Germany, 16–20 September 1996* (ed. R Vollmar, W Erhard, V Jossifov), pp. 287–290. Berlin, Germany: Springer.
18. Adamatzky A, Costello BDL, Asai T 2005 *Reaction-diffusion computers*. Amsterdam, The Netherlands: Elsevier.
19. Adamatzky A. 2002 On dynamics of affective liquids. *Dyn. Psychol.* **1**, pp. 1–12.
20. Adamatzky A, de Lacy Costello B, Melhuish C, Ratcliffe N. 2003 Liquid brains for robots. *AISB Q.* **112**, 5.
21. Adamatzky A, Holland O, Rambidi N, Winfield A. 1999 Wet artificial brains: towards the chemical control of robot motion by reaction-diffusion and excitable media. In *Proc. 5th Eur. Conf. Advances in Artificial Life, ECAL'99, Lausanne, Switzerland, 13–17 September 1999* (ed. D Floreano, J-D Nicoud, F Mondada), pp. 304–313. Berlin, Germany: Springer.
22. Adamatzky A. 2005 Parachemistry of mind: case studies of doxastic and affective mixtures. In *Visions of mind: architectures for cognition and affect* (ed. DN Davis), pp. 1–20. Hershey, PA: IGI Global.
23. Adamatzky A. 2005 Non-linear dynamics in affective solutions: analysis of massive collectives of

emotional agents. *Kybernetes* **34**, 652–665. (doi:10.1108/03684920510595346)

24. Emch A. 1901 Two hydraulic methods to extract the *n*th root of any number. *Am. Math. Month.* **8**, 10–12. (doi:10.1080/00029890.1901.12000520)
25. Frame J. 1945 Machines for solving algebraic equations. *Math. Comput.* **1**, 337–353. (doi:10.1090/S0025-5718-1945-0011196-2)
26. Gibb D. 1914 The instrumental solution of numerical equations. In *Modern instruments and methods of calculation: a handbook of the Napier Tercentenary Exhibition* (ed. EM Horsburgh), pp. 259–268. Edinburgh, UK: Royal Society of Edinburgh.
27. Luk'yanov V. 1939 Hydraulic instruments for technical calculations. *Izv. Akad. Nauk SSSR* **2**, pp. 34–56.
28. Moore A. 1936 The hydrocal. *Ind. Eng. Chem.* **28**, 704–708. (doi:10.1021/ie50318a022)
29. Bissell C. 2007 Historical perspectives - the Moniac a hydromechanical analog computer of the 1950s. *IEEE Control Syst.* **27**, 69–74. (doi:10.1109/MCS.2007.284511)
30. Moore A. 1949 Fields from fluid flow mappers. *J. Appl. Phys.* **20**, 790–804. (doi:10.1063/1.1698529)
31. Tesla N. 1920 *Valvular conduit*. US Patent no. 1,329,559.
32. Bowles RE. 1965 *Passive pure fluid component*. US Patent no. 3,191,623.
33. Drake RT, Gehring JAJ, Marvin J. 2006 *Pure fluid computer*. US Patent no. 3,190,554.
34. Hobbs EV. 1963 Fluid amplification. 9. Logic elements. Technical report no. TR-1114. Washington, DC: Harry Diamond Laboratories.
35. Pul FW. 1969 Fluid mechanics of the momentum flueric diode. In *Proc. IFAC Symp. Fluidics*, vol. 1, pp. 1–15. London: Royal Aeronautical Society.
36. Bauer P. 1965 "and" gate. US Patent no. 3,191,611.
37. Agladze K, Aliev R, Yamaguchi T, Yoshikawa K. 1996 Chemical diode. *J. Phys. Chem.* **100**, 13 895–13 897. (doi:10.1021/jp9608990)
38. Gorecki J, Yoshikawa K, Igarashi Y. 2003 On chemical reactors that can count. *J. Phys. Chem. A* **107**, 1664–1669. (doi:10.1021/jp021041f)
39. Kuhnert L, Agladze K, Krinsky V. 1989 Image processing using light-sensitive chemical waves. *Nature* **337**, 244–247. (doi:10.1038/337244a0)
40. Steinbock O, Kettunen P, Showalter K. 1996 Chemical wave logic gates. *J. Phys. Chem.* **100**, 18 970–18 975. (doi:10.1021/jp961209v)
41. Adamatzky A. 1994 Constructing a discrete generalized Voronoi diagram in reaction-diffusion media. *Neural Netw. World* **6**, 635–643.
42. Adamatzky A. 1996 Reaction-diffusion computer: massively parallel molecular computation. *Math. Res.* **96**, 287–290.
43. Adamatzky A, Tolmachiev D. 1997 Chemical processor for computation of skeleton of planar shape. *Adv. Mater. Opt. Electron.* **7**, 135–139. (doi:10.1002/(ISSN)1099-0712)
44. Tolmachiev D, Adamatzky A. 1996 Chemical processor for computation of Voronoi diagram. *Adv. Funct. Mater.* **6**, 191–196. (doi:10.1002/(SICI)1099-0712(199607)6:4<191::AID-AMO0238>3.0.CO;2-G)
45. Adamatzky A, de Lacy Costello B, Melhuish C, Ratcliffe N. 2004 Experimental implementation of mobile robot taxis with onboard Belousov–Zhabotinsky chemical medium. *Mater. Sci. Eng. C* **24**, 541–548. (doi:10.1016/j.msec.2004.02.002)
46. Fuerstman MJ, Deschatelets P, Kane R, Schwartz A, Kenis PJ, Deutch JM, Whitesides GM. 2003 Solving mazes using microfluidic networks. *Langmuir* **19**, 4714–4722. (doi:10.1021/la030054x)
47. Cheow LF, Yobas L, Kwong D-L. 2007 Digital microfluidics: droplet based logic gates. *Appl. Phys. Lett.* **90**, 054107. (doi:10.1063/1.2435607)
48. Fair RB. 2007 Digital microfluidics: is a true lab-on-a-chip possible? *Microfluid. Nanofluid.* **3**, 245–281. (doi:10.1007/s10404-007-0161-8)
49. Prakash M, Gershenfeld N. 2007 Microfluidic bubble logic. *Science* **315**, 832–835. (doi:10.1126/science.1136907)
50. Toepke MW, Abhyankar VV, Beebe DJ. 2007 Microfluidic logic gates and timers. *Lab. Chip* **7**, 1449–1453. (doi:10.1039/b708764k)
51. Čejková J, Novák M, Štěpánek F, Hanczyc MM. 2014 Dynamics of chemotactic droplets in salt concentration gradients. *Langmuir* **30**, 11 937–11 944. (doi:10.1021/la502624f)
52. Lagzi I, Soh S, Wesson PJ, Browne KP, Grzybowski BA. 2010 Maze solving by chemotactic droplets. *J. Am. Chem. Soc.* **132**, 1198–1199. (doi:10.1021/ja9076793)
53. Mertaniemi H, Forchheimer R, Ikkala O, Ras RH. 2012 Rebounding droplet-droplet collisions on superhydrophobic surfaces: from the phenomenon to droplet logic. *Adv. Mater.* **24**, 5738–5743. (doi:10.1002/adma.v24.42)
54. Draper TC, Fullarton C, Phillips N, de Lacy Costello BP, Adamatzky A. 2017 Liquid marble interaction gate for collision-based computing. *Mater. Today* **20**, 561–568. (doi:10.1016/j.mattod.2017.09.004)
55. Arlazorov M. 1952 Mashina s vysshem obrazovaniem [A machine with higher education]. *Ogoniok* **31** (in Russian).
56. The Polytechnic Museum. 2018 Online exhibition. Water computer (in Russian). See https://polymus.ru/ru/museum/fonds/tours/vodyanoy-kompyuter#virt-tour-item-4.
57. Hele-Shaw HS, Hay A. 1900 Lines of induction in a magnetic field. *Proc. R. Soc. Lond.* **67**, 234–236.
58. Hele-Shaw H, Hay A, Powell P. 1905 Hydrodynamical and electromagnetic investigations regarding the magnetic-flux distribution in toothed core armatures. *J. Inst. Electr. Eng.* **34**, 21–37. (doi:10.1049/jiee-1.1905.0001)
59. Moore A. 2018 Arthur D. Moore papers: 1916–1984. See https://quod.lib.umich.edu/b/bhlead/umich-bhl-851959?view=text (accessed June 2018).
60. McFee R, Stow RM, Johnston FD. 1952 Graphic representation of electrocardiographic leads by means of fluid mappers. *Circulation* **6**, 21–29. (doi:10.1161/01.CIR.6.1.21)
61. Clem JD. 1954 The use of the fluid mapper in an investigation of flow into symmetrical openings obstructed by plane surfaces. PhD thesis, Georgia Institute of Technology.
62. Adamatzky A. 2017 Physical maze solvers. all twelve prototypes implement 1961 LEE algorithm. In *Emergent computation* (ed. A. Adamatzky), pp. 489–504. Berlin, Germany: Springer.
63. Golovin A, Gupalo I, Riazantsev I. 1986 O khemotermokapilliarnom effekte dlia dvizheniia kapli v zhidkosti [The chemothermocapillary effect for drop motion in a fluid]. *Akad. Nauk SSSR, Dok.* **290**, 35–39 (in Russian.)
64. Golovin A, Ryazantsev YS. 1990 The drift of reacting drop owing to chemosolutocapillary effect. *Izv. Akad. Nauk SSSR, Mekh. Zhidk. Gaza* **3**, 23–27.
65. Levich VG. 1963 *Physicochemical hydrodynamics*. Englewood Cliffs, NJ: Prentice-Hall.
66. Velarde MG. 1998 Drops, liquid layers and the Marangoni effect. *Phil. Trans. R. Soc. Lond. A* **356**, 829–842. (doi:10.1098/rsta.1998.0190)
67. Yoshinaga N. 2014 Spontaneous motion and deformation of a self-propelled droplet. *Phys. Rev. E* **89**, 012913. (doi:10.1103/PhysRevE.89.012913)
68. Young N, Goldstein J, Block MJ. 1959 The motion of bubbles in a vertical temperature gradient. *J. Fluid Mech.* **6**, 350–356. (doi:10.1017/S0022112059000684)
69. Čejková J, Banno T, Hanczyc MM, Štěpánek F. 2017 Droplets as liquid robots. *Artif. Life* **23**, 528–549. (doi:10.1162/ARTL_a_00243)
70. Chiolerio A, Quadrelli MB. 2017 Smart fluid systems: the advent of autonomous liquid robotics. *Adv. Sci.* **4**, 1700036. (doi:10.1002/advs.v4.7)
71. Adamatzky A. 2012 Slime mold solves maze in one pass, assisted by gradient of chemo-attractants. *IEEE Trans. Nanobioscience* **11**, 131–134. (doi:10.1109/TNB.2011.2181978)
72. Ricigliano V, Chitaman J, Tong J, Adamatzky A, Howarth DG. 2015 Plant hairy root cultures as plasmodium modulators of the slime mold emergent computing substrate *Physarum polycephalum*. *Front. Microbiol.* **6**, 720. (doi:10.3389/fmicb.2015.00720)
73. Conway A 1971 *Guide to fluidics*. London, UK: Macdonald & Co. (Publishers).
74. Kirshner JM, Katz S 1975 *Design theory of fluidic components*. New York, NY: Academic Press.
75. Moylan MJ 1968 *Fluid logic in simple terms*. London, UK: Machinery Publishing Co.
76. Belsterling CA 1971 *Fluidic systems design*. New York, NY: John Wiley & Sons.
77. Dummer GWA, Robertson JM. 2013 *Fluidic components and equipment 1968–9: Pergamon electronics data series*. Amsterdam, The Netherlands; Elsevier.
78. Gunji G *et al.* 2011 Embodied swarming based on back propagation through time shows water-crossing, hourglass and logic-gate behaviors. In *ECAL* (ed. T Lenaerts, M Giacobini, H Bersini, P Bourgine, M Dorigo, R Doursat), pp. 294–301. Paris, France: Springer.

79. Gunji Y-P, Nishiyama Y, Adamatzky A. 2011 Robust soldier crab ball gate. *Complex Syst.* **20**, 2. pp. 93–104.
80. Nishiyama Y, Gunji Y-P, Adamatzky A. 2013 Collision-based computing implemented by soldier crab swarms. *Int. J. Parallel Emergent Distrib. Syst.* **28**, 67–74. (doi:10.1080/17445760.2012.662682)
81. Adamatzky A, Harding S, Erokhin V, Mayne R, Gizzie N, Baluška F, Mancuso S, Sirakoulis GC. 2018 Computers from plants we never made: speculations. In *Inspired by nature* (ed. A Adamatzky), pp. 357–387. Berlin, Germany: Springer.
82. Adamatzky A, Sirakoulis GC, Martinez GJ, Baluška F, Mancuso S. 2017 On plant roots logical gates. *BioSystems* **156**, 40–45. (doi:10.1016/j.biosystems.2017.04.002)
83. Nishiyama Y, Gunji Y-P, Adamatzky A. 2013 Collision-based computing implemented by soldier crab swarms. *Int. J. Parallel Emergent Distrib. Syst.* **28**, 67–74. (doi:10.1080/17445760.2012.662682)
84. Ciszak M, Comparini D, Mazzolai B, Baluška F, Arecchi FT, Vicsek T, Mancuso S. 2012 Swarming behavior in plant roots. *PLoS ONE* **7**, e29759. (doi:10.1371/journal.pone.0029759)
85. Morgan AJ, Barrow DA, Adamatzky A, Hanczyc MM. 2016 Simple fluidic digital half-adder. See http://arxiv.org/abs/1602.01084.
86. Fredkin E, Toffoli T. 2002 Conservative logic. In *Collision-based computing* (ed. A Adamatzky). Berlin, Germany: Springer.
87. Adamatzky A, de Lacy Costello B. 2002 Collision-free path planning in the Belousov–Zhabotinsky medium assisted by a cellular automaton. *Naturwissenschaften* **89**, 474–478. (doi:10.1007/s00114-002-0363-6)
88. Rabe C, Malet J, Feuillebois F. 2010 Experimental investigation of water droplet binary collisions and description of outcomes with a symmetric Weber number. *Phys. Fluids* **22**, 047101. (doi:10.1063/1.3392768)
89. Ashgriz N, Poo J. 1990 Coalescence and separation in binary collisions of liquid drops. *J. Fluid Mech.* **221**, 183–204. (doi:10.1017/S0022112090003536)
90. Aussillous P, Quéré D. 2001 Liquid marbles. *Nature* **411**, 924–927. (doi:10.1038/35082026)
91. Draper TC, Fullarton C, Phillips N, de Lacy Costello BP, Adamatzky A. 2018 Mechanical sequential counting with liquid marbles. In *Proc. Int. Conf. Unconventional Computation and Natural Computation* (ed. S Stepney, S Verlan), pp. 59–71. Berlin, Germany: Springer.
92. Adamatzky A, de Lacy Costello B. 2016 Computing with liquid marbles. EPSRC grant EP/P016677/1. See https://gow.epsrc.ukri.org/NGBOViewGrant.aspx?GrantRef=EP/P016677/1.
93. Godfrey JT. 1968 *Binary digital computer*. US Patent no. 3,390,471.
94. Bormashenko E, Bormashenko Y, Grynyov R, Aharoni H, Whyman G, Binks BP. 2015 Self-propulsion of liquid marbles: Leidenfrost-like levitation driven by Marangoni flow. *J. Phys. Chem. C* **119**, 9910–9915. (doi:10.1021/acs.jpcc.5b01307)
95. Ooi CH, van Nguyen A, Evans GM, Gendelman O, Bormashenko E, Nguyen N-T. 2015 A floating self-propelling liquid marble containing aqueous ethanol solutions. *RSC Adv.* **5**, 101006–101012. (doi:10.1039/C5RA23946J)
96. Paven M, Mayama H, Sekido T, Butt H-J, Nakamura Y, Fujii S. 2016 Light-driven delivery and release of materials using liquid marbles. *Adv. Funct. Mater.* **26**, 3199–3206. (doi:10.1002/adfm.201600034)
97. Burr HS, Lane C. 1935 Electrical characteristics of living systems. *Yale J. Biol. Med.* **8**, 31–35.
98. Buzsaki G 2006 *Rhythms of the brain*. Oxford, UK: Oxford University Press.
99. Levin M. 2007 Large-scale biophysics: ion flows and regeneration. *Trends Cell Biol.* **17**, 261–270. (doi:10.1016/j.tcb.2007.04.007)
100. Baluška F, Mancuso S. 2013 Root apex transition zone as oscillatory zone. *Front. Plant Sci.* **4**, 354. (doi:10.3389/fpls.2013.00354)
101. Baluška F, Mancuso S, Volkmann D, Barlow P. 2010 Root apex transition zone: a signalling-response nexus in the root. *Trends Plant Sci.* **15**, 402–408. (doi:10.1016/j.tplants.2010.04.007)
102. Brenner E, Stahlberg R, Mancuso S, Vivanco J, Baluška F, Van Volkenburgh E. 2006 Plant neurobiology: an integrated view of plant signaling. *Trends Plant Sci.* **11**, 413–419. (doi:10.1016/j.tplants.2006.06.009)
103. Fromm J, Lautner S. 2007 Electrical signals and their physiological significance in plants. *Plant Cell Environ.* **30**, 249–257. (doi:10.1111/j.1365-3040.2006.01614.x)
104. Gagliano M, Renton M, Depczynski M, Mancuso S. 2014 Experience teaches plants to learn faster and forget slower in environments where it matters. *Oecologia* **175**, 63–72. (doi:10.1007/s00442-013-2873-7)
105. Mancuso S. 1999 Hydraulic and electrical transmission of wound-induced signals in *Vitis vinifera*. *Aust. J. Plant Physiol.* **26**, 55–61. (doi:10.1071/PP98098)
106. Mancuso S. 2000 Electrical resistance changes during exposure to low temperature measure chilling and freezing tolerance in olive tree (*Olea europaea* L.) plants. *Plant Cell Environ.* **23**, 291–299. (doi:10.1046/j.1365-3040.2000.00540.x)
107. Masi E *et al.* 2009 Spatiotemporal dynamics of the electrical network activity in the root apex. *Proc. Natl Acad. Sci. USA* **106**, 4048–4053. (doi:10.1073/pnas.0804640106)
108. Shabala S, Shabala L, Gradmann D, Chen Z, Newman I, Mancuso S. 2006 Oscillations in plant membrane transport: model predictions, experimental validation, and physiological implications. *J. Exp. Bot.* **57**, 171–184. (doi:10.1093/jxb/erj022)
109. Achenbach U, Wohlfarth-Bottermann K. 1981 Synchronization and signal transmission in protoplasmic strands of *Physarum* - effects of externally applied substances and mechanical influences. *Planta* **151**, 574–583. (doi:10.1007/BF00387437)
110. Adamatzky A, Jones J. 2011 On electrical correlates of *Physarum polycephalum* spatial activity: can we see *Physarum* machine in the dark? *Biophys. Rev. Lett.* **6**, 29–57. (doi:10.1142/S1793048011001257)
111. Alonso S, Strachauer U, Radszuweit M, Bʹar M, Hauser M. 2016 Oscillations and uniaxial mechanochemical waves in a model of an active poroelastic medium: application to deformation patterns in protoplasmic droplets of *Physarum polycephalum*. *Physica D* **318–319**, 58–69. (doi:10.1016/j.physd.2015.09.017)
112. Ebine M. 2014 Estimation of plasmodial activity in response to electrical stimulation and the potential use of this measurement as an environmental indicator: the correlation between galvanotaxis and ATP levels in the plasmodium. *IEEJ Trans. Electron. Inf. Syst.* **134**, 1755–1759. (doi:10.1541/ieejeiss.134.1755)
113. Häder D. 1985 Role of calcium in phototaxis of *Physarum polycephalum*. *Plant Cell Physiol.* **26**, 1411–1417.
114. Radszuweit M, Engel H, Barr M. 2011 A model for oscillations and pattern formation in protoplasmic droplets of *Physarum polycephalum*. *Eur. Phys. J. Spec. Top.* **191**, 159–172. (doi:10.1140/epjst/e2010-01348-2)
115. Whiting J, de Lacy Costello B, Adamatzky A. 2014 Towards slime mould chemical sensor: mapping chemical inputs onto electrical potential dynamics of *Physarum polycephalum*. *Sens. Actuators B* **191**, 844–853. (doi:10.1016/j.snb.2013.10.064)
116. Adamatzky A. 2018 On spiking behaviour of oyster fungi *Pleurotus djamor*. *Sci. Rep.* **8**, 7873. (doi:10.1038/s41598-018-26007-1)
117. Slayman C, Scott Long W, Gradmann D. 1976 'Action potentials' in *Neurospora crassa*, a mycelial fungus. *BBA Biomembranes* **426**, 732–744. (doi:10.1016/0005-2736(76)90138-3)
118. Jaffe L. 2010 Fast calcium waves. *Cell Calcium* **48**, 102–113. (doi:10.1016/j.ceca.2010.08.007)
119. Malho R, Moutinho A, van der Luit A, Trewavas A. 1998 Spatial characteristics of calcium signalling: the calcium wave as a basic unit in plant cell calcium signalling. *Phil. Trans. R. Soc. B* **353**, 1463–1473. (doi:10.1098/rstb.1998.0302)
120. Nakamura A, Kohama K. 1999 Calcium regulation of the actin-myosin interaction of *Physarum polycephalum*. *Int. Rev. Cytol.* **191**, 53–98. (doi:10.1016/S0074-7696(08)60157-6)
121. Ng C-Y, Mcainsh M. 2003 Encoding specificity in plant calcium signalling: hot-spotting the ups and downs and waves. *Ann. Bot.* **92**, 477–485. (doi:10.1093/aob/mcg173)
122. Ranty B, Cotelle V, Galaud J-P, Mazars C. 2012 Nuclear calcium signaling and its involvement in transcriptional regulation in plants. *Adv. Exp. Med. Biol.* **740**, 1123–1143. (doi:10.1007/978-94-007-2888-2)
123. Stephan A, Schroeder J. 2014 Plant salt stress status is transmitted systemically via propagating calcium

waves. *Proc. Natl Acad. Sci. USA* **111**, 6126–6127. (doi:10.1073/pnas.1404895111)

124. Teplov V. 2017 Role of mechanics in the appearance of oscillatory instability and standing waves of the mechanochemical activity in the *Physarum polycephalum* plasmodium. *J. Phys. D Appl. Phys.* **50**, 213002. (doi:10.1088/1361-6463/aa6727)
125. Yoshiyama S, Ishigami M, Nakamura A, Kohama K. 2010 Calcium wave for cytoplasmic streaming of *Physarum polycephalum*. *Cell Biol. Int.* **34**, 35–40.
126. Adamatzky A. 2011 Topics in reaction-diffusion computers. *J. Comput. Theor. Nanosci.* **8**, 295–303. (doi:10.1166/jctn.2011.1693)
127. Adamatzky A. 2012 Reaction-diffusion computing. In *Computational complexity: theory, techniques, and applications*, pp. 2594–2610. New York, NY: Springer.
128. Belousov B. 1959 Periodicheski dejstvuijuschaja reakcia [periodically acting reaction and its mechanism]. *Sbornik referatov po radiatsionnoj medicine* [*Collection of reports on radioactive medicine*] **147**, 145 (in Russian.)
129. Zaikin A, Zhabotinsky A. 1970 Concentration wave propagation in two-dimensional liquid-phase self-oscillating system. *Nature* **225**, 535–537. (doi:10.1038/225535b0)
130. Zhabotinsky AM. 1964 Periodical oxidation of malonic acid in solution (a study of the Belousov reaction kinetics). *Biofizika* **9**, 306–311.
131. Yokoi H, Adamatzky A, de Lacy Costello B, Melhuish C. 2004 Excitable chemical medium controller for a robotic hand: closed-loop experiments. *Int. J. Bifurcation Chaos* **14**, 3347–3354. (doi:10.1142/S0218127404011363)
132. Kuhnert L. 1986 A new optical photochemical memory device in a light-sensitive chemical active medium. *Nature* **319**, 393. (doi:10.1038/319393a0)
133. Agladze K, Obata S, Yoshikawa K. 1995 Phase-shift as a basis of image processing in oscillating chemical medium. *Physica D* **84**, 238–245. (doi:10.1016/0167-2789(95)00029-4)
134. Aliev RR. 1994 Oscillation phase dynamics in the Belousov-Zhabotinsky reaction. Implementation to image processing. *J. Phys. Chem.* **98**, 3999–4002. (doi:10.1021/j100066a016)
135. Rambidi N, Kuular T-O, Makhaeva E. 1998 Information-processing capabilities of chemical reaction–diffusion systems. 1. Belousov–Zhabotinsky media in hydrogel matrices and on solid supports. *Adv. Mater. Opt. Electron.* **8**, 163–171. (doi:10.1002/(ISSN)1099-0712)
136. Rambidi N, Shamayaev K, Peshkov GY. 2002 Image processing using light-sensitive chemical waves. *Phys. Lett. A* **298**, 375–382. (doi:10.1016/S0375-9601(02)00583-2)
137. Rambidi NG. 2005 Biologically inspired information processing technologies: reaction-diffusion paradigm. *Int. J. Unconv. Comput.* **1**, 101–120.
138. Sielewiesiuk J, Górecki J. 2001 Logical functions of a cross junction of excitable chemical media. *J. Phys. Chem. A* **105**, 8189–8195. (doi:10.1021/jp011072v)
139. Costello BDL, Adamatzky A, Jahan I, Zhang L. 2011 Towards constructing one-bit binary adder in excitable chemical medium. *Chem. Phys.* **381**, 88–99. (doi:10.1016/j.chemphys.2011.01.014)
140. Zhang G-M, Wong I, Chou M-T, Zhao X. 2012 Towards constructing multi-bit binary adder based on Belousov–Zhabotinsky reaction. *J. Chem. Phys.* **136**, 164108. (doi:10.1063/1.3702846)
141. Sun M-Z, Zhao X. 2013 Multi-bit binary decoder based on Belousov–Zhabotinsky reaction. *J. Chem. Phys.* **138**, 114106. (doi:10.1063/1.4794995)
142. Motoike IN, Adamatzky A. 2005 Three-valued logic gates in reaction–diffusion excitable media. *Chaos Solitons Fractals* **24**, 107–114. (doi:10.1016/S0960-0779(04)00461-8)
143. Stevens WM, Adamatzky A, Jahan I, de Lacy Costello B. 2012 Time-dependent wave selection for information processing in excitable media. *Phys. Rev. E* **85**, 066129. (doi:10.1103/PhysRevE.85.066129)
144. Sendiña-Nadal I, Mihaliuk E, Wang J, Pérez-Muñuzuri V, Showalter K. 2001 Wave propagation in subexcitable media with periodically modulated excitability. *Phys. Rev. Lett.* **86**, 1646–1649. (doi:10.1103/PhysRevLett.86.1646)
145. Adamatzky A. 2004 Collision-based computing in Belousov–Zhabotinsky medium. *Chaos Solitons Fractals* **21**, 1259–1264. (doi:10.1016/j.chaos.2003.12.068)
146. Adamatzky A, de Lacy Costello B. 2007 Binary collisions between wave-fragments in a sub-excitable Belousov–Zhabotinsky medium. *Chaos Solitons Fractals* **34**, 307–315. (doi:10.1016/j.chaos.2006.03.095)
147. Costello BDL, Adamatzky A. 2005 Experimental implementation of collision-based gates in Belousov–Zhabotinsky medium. *Chaos Solitons Fractals* **25**, 535–544. (doi:10.1016/j.chaos.2004.11.056)
148. de Lacy Costello B, Toth R, Stone C, Adamatzky A, Bull L. 2009 Implementation of glider guns in the light-sensitive Belousov–Zhabotinsky medium. *Phys. Rev. E* **79**, 026114. (doi:10.1103/PhysRevE.79.026114)
149. Toth R, Stone C, de Lacy Costello B, Adamatzky A, Bull L. 2010 Simple collision-based chemical logic gates with adaptive computing. In *Theoretical and technological advancements in nanotechnology and molecular computation: interdisciplinary gains* (ed. B MacLennan), p. 162. New York, NY: Nova Science Publishers.
150. Agladze K, Magome N, Aliev R, Yamaguchi T, Yoshikawa K. 1997 Finding the optimal path with the aid of chemical wave. *Physica D* **106**, 247–254. (doi:10.1016/S0167-2789(97)00049-3)
151. Rambidi N, Yakovenchuk D. 2001 Chemical reaction-diffusion implementation of finding the shortest paths in a labyrinth. *Phys. Rev. E* **63**, 026607. (doi:10.1103/PhysRevE.63.026607)
152. Steinbock A, Tóth Á, Showalter K. 1995 Navigating complex labyrinths: optimal paths from chemical waves. *Science* **267**, 868–871. (doi:10.1126/science.267.5199.868)
153. Adamatzky A, Dehshibi MM. 2018 Exploring Tehran with excitable medium. See http://arxiv.org/abs/1807.09023.
154. Adamatzky A, Phillips N, Weerasekera R, Tsompanas M-A, Sirakoulis GC. 2018 Street map analysis with excitable chemical medium. *Phys. Rev. E* **98**, 012306. (doi:10.1103/PhysRevE.98.012306)
155. Litschel T, Norton MM, Tserunyan V, Fraden S. 2018 Engineering reaction–diffusion networks with properties of neural tissue. *Lab. Chip* **18**, 714–722. (doi:10.1039/C7LC01187C)
156. Murase Y, Maeda S, Hashimoto S, Yoshida R. 2008 Design of a mass transport surface utilizing peristaltic motion of a self-oscillating gel. *Langmuir* **25**, 483–489. (doi:10.1021/la8029006)
157. Balazs AC, Aizenberg J. 2014 Reconfigurable soft matter. *Soft Matter* **10**, 1244–1245. (doi:10.1039/c4sm90006e)
158. Yoshida R. 2010 Self-oscillating gels driven by the Belousov–Zhabotinsky reaction as novel smart materials. *Adv. Mater.* **22**, 3463–3483. (doi:10.1002/adma.200904075)
159. Adamatzky A. 2015 Binary full adder, made of fusion gates, in a subexcitable Belousov–Zhabotinsky system. *Phys. Rev. E* **92**, 032811. (doi:10.1103/PhysRevE.92.032811)
160. Adamatzky A, Holley J, Dittrich P, Gorecki J, Costello BDL, Zauner K-P, Bull L. 2012 On architectures of circuits implemented in simulated Belousov–Zhabotinsky droplets. *BioSystems* **109**, 72–77. (doi:10.1016/j.biosystems.2011.12.007)
161. Adamatzky A. 2017 Fredkin and Toffoli gates implemented in Oregonator model of Belousov–Zhabotinsky medium. *Int. J. Bifurcation Chaos* **27**, 1750041. (doi:10.1142/S0218127417500419)
162. Costello BDL, Jahan I, Ahearn M, Holley J, Bull L, Adamatzky A. 2012 Initiation of waves in BZ encapsulated vesicles using light-towards design of computing architectures. See http://arxiv.org/abs/1212.2244.
163. Delgado J, Li N, Leda M, González-Ochoa HO, Fraden S, Epstein IR. 2011 Coupled oscillations in a 1D emulsion of Belousov–Zhabotinsky droplets. *Soft Matter* **7**, 3155–3167. (doi:10.1039/c0sm01240h)
164. Tomasi R, Noël J-M, Zenati A, Ristori S, Rossi F, Cabuil V, Kanoufi F, Abou-Hassan A. 2014 Chemical communication between liposomes encapsulating a chemical oscillatory reaction. *Chem. Sci.* **5**, 1854–1859. (doi:10.1039/C3SC53227E)
165. Torbensen K, Rossi F, Ristori S, Abou-Hassan A. 2017 Chemical communication and dynamics of droplet emulsions in networks of Belousov–Zhabotinsky micro-oscillators produced by microfluidics. *Lab. Chip* **17**, 1179–1189. (doi:10.1039/C6LC01583B)
166. Vanag VK. 2004 Waves and patterns in reaction–diffusion systems. Belousov–Zhabotinsky reaction in water-in-oil microemulsions. *Phys. Usp.* **47**, 923–941. (doi:10.1070/PU2004v047n09ABEH001742)
167. Vanag VK, Epstein IR. 2011 Excitatory and inhibitory coupling in a one-dimensional array of Belousov-Zhabotinsky micro-oscillators: theory.

Phys. Rev. E **84**, 066209. (doi:10.1103/PhysRevE.84.066209)

168. Vanag VK, Hanazaki I. 1996 pH dependence of the Belousov–Zhabotinsky reaction in water-in-oil reverse microemulsion of AOT in octane. *J. Phys. Chem.* **100**, 10 609–10 614. (doi:10.1021/jp953063q)
169. Gruenert G, Gizynski K, Escuela G, Ibrahim B, Gorecki J, Dittrich P. 2015 Understanding networks of computing chemical droplet neurons based on information flow. *Int. J. Neural Syst.* **25**, 1450032. (doi:10.1142/S0129065714500324)
170. Kaminaga A, Vanag VK, Epstein IR. 2006 A reaction–diffusion memory device. *Angew. Chem. Int. Ed.* **45**, 3087–3089. (doi:10.1002/(ISSN)1521-3773)
171. Wang A, Gold J, Tompkins N, Heymann M, Harrington K, Fraden S. 2016 Configurable NOR gate arrays from Belousov-Zhabotinsky micro-droplets. *Eur. Phys. J. Spec. Top.* **225**, 211–227. (doi:10.1140/epjst/e2016-02622-y)
172. Fullarton C, Draper TC, Phillips N, Costello BP, Adamatzky A. 2018 Belousov–Zhabotinsky reaction in liquid marbles. See http://arxiv.org/abs/1806.07181.
173. Adamatzky A, de Lacy Costello B, Bull L. 2011 On polymorphic logical gates in subexcitable chemical medium. *Int. J. Bifurcation Chaos* **21**, 1977–1986. (doi:10.1142/S0218127411029574)
174. Adamatzky A, de Lacy Costello B, Dittrich P, Gorecki J, Zauner K-P. 2014 On logical universality of Belousov–Zhabotinsky vesicles. *Int. J. Gen. Syst.* **43**, 757–769. (doi:10.1080/03081079.2014.921000)
175. Holley J, Adamatzky A, Bull L, Costello BDL, Jahan I. 2011 Computational modalities of Belousov–Zhabotinsky encapsulated vesicles. *Nano Commun. Netw.* **2**, 50–61. (doi:10.1016/j.nancom.2011.02.002)
176. Holley J, Jahan I, Costello BDL, Bull L, Adamatzky A. 2011 Logical and arithmetic circuits in Belousov–Zhabotinsky encapsulated disks. *Phys. Rev. E* **84**, 056110. (doi:10.1103/PhysRevE.84.056110)
177. Gorecki J, Gorecka J, Adamatzky A. 2014 Information coding with frequency of oscillations in Belousov–Zhabotinsky encapsulated disks. *Phys. Rev. E* **89**, 042910. (doi:10.1103/PhysRevE.89.042910)
178. Gizynski K, Gruenert G, Dittrich P, Gorecki J. 2017 Evolutionary design of classifiers made of droplets containing a nonlinear chemical medium. *Evol. Comput.* **25**, 643–671. (doi:10.1162/evco_a_00197)
179. Adamatzky A, de Lacy Costello B, Ratcliffe NM. 2002 Experimental reaction–diffusion pre-processor for shape recognition. *Phys. Lett. A* **297**, 344–352. (doi:10.1016/S0375-9601(02)00289-X)
180. de Lacy Costello B, Ratcliffe N, Adamatzky A, Zanin AL, Liehr AW, Purwins H-G. 2004 The formation of Voronoi diagrams in chemical and physical systems: experimental findings and theoretical models. *Int. J. Bifurcation Chaos* **14**, 2187–2210. (doi:10.1142/S021812740401059X)
181. Margolus N, Levitin LB. 1998 The maximum speed of dynamical evolution. *Physica D* **120**, 188–195. (doi:10.1016/S0167-2789(98)00054-2)
182. Zheng R, Gao J, Wang J, Chen G. 2011 Reversible temperature regulation of electrical and thermal conductivity using liquid–solid phase transitions. *Nat. Commun.* **2**, 289. (doi:10.1038/ncomms1288)
183. Wissman J, Dickey MD, Majidi C. 2017 Field-controlled electrical switch with liquid metal. *Adv. Sci.* **4**, 1700169. (doi:10.1002/advs.201700169)
184. Kim DY, Herman S, Steckl AJ. 2008 IV and gain characteristics of electrowetting-based liquid field effect transistor. In *Proc. 17th Biennial University/Government/Industry Micro/Nano Symp., 2008. UGIM 2008*, pp. 2–5. Louisville, KY: IEEE Press.
185. Ren H, Wu S-T. 2010 Optical switch using a deformable liquid droplet. *Opt. Lett.* **35**, 3826–3828. (doi:10.1364/OL.35.003826)
186. Taft C. 1967 Hydraulic fluidics. Technical report. Warrendale, PA: SAE.
187. Ball R. 1974 *Nuclear reactor control system*. US Patent no. 3,793,141.
188. Lee S-S, Kim S-H, Suh K-Y. 2009 The design features of the advanced power reactor 1400. *Nucl. Eng. Technol.* **41**, 995–1004. (doi:10.5516/NET.2009.41.8.995)
189. Takayama S, Mosadegh B. 2011 *Microfluidic control systems*. US Patent App. no. 13/119,359.
190. Magill J, McManus K. 1998 Control of dynamic stall using pulsed vortex generator jets. In *Abstr. 36th AIAA Aerospace Sciences Meeting and Exhibit*, Reno, NV, USA, 12–15 January 1998, p. 675.
191. Shmilovich A, Kent SR. 2016 *Fluidic traverse actuator*. US Patent no. 9,511,849.
192. Tang WC, Lee AP. 2001 Defense applications of MEMS. *MRS Bull.* **26**, 318–319. (doi:10.1557/mrs2001.70)
193. Mazzolai B, Mattoli V. 2016 Robotics: generation soft. *Nature* **536**, 400–401. (doi:10.1038/536400a)
194. Chang Y-H, Lee G-B, Huang F-C, Chen Y-Y, Lin J-L. 2006 Integrated polymerase chain reaction chips utilizing digital microfluidics. *Biomed. Microdevices* **8**, 215–225. (doi:10.1007/s10544-006-8171-y)
195. Cho SK, Moon H, Kim C-J. 2013 Creating, transporting, cutting, and merging liquid droplets by electrowetting-based actuation for digital microfluidic circuits. *J. Microelectromech. Syst.* **12**, 70–80.
196. Su F, Hwang W, Chakrabarty K. 2006 Droplet routing in the synthesis of digital microfluidic biochips. In *DATE '06. Proc. Conf. Design, Automation and Test in Europe, Munich, Germany, 6–10 March 2006* (ed. G Gielen), vol. 1, pp. 323–328. Leuven, Belgium: European Design and Automation Association.